Numerical Investigation of Multi-compartment Fire Scenarios using Large Eddy Simulation (LES)

by

Duy Quang Le

A thesis
presented to the University of Waterloo
in fulfillment of the
thesis requirement for the degree of
Master of Applied Science
in
Mechanical Engineering

Waterloo, Ontario, Canada, 2016

Author's Declaration

I hereby declare that I am the sole author of this thesis. This is a true copy of the thesis, including any required final revisions, as accepted by my examiners.

I understand that my thesis may be made electronically available to the public.

Abstract

The selected fire scenario corresponds to the Propagation d'un Incendie pour des Scénarios Multi-locaux Elémentaires (PRISME) Integral Test 4, which is a multi-room configuration with a single pool fire burning Hydrogenated Tetra-Propylene (HTP) fuel and fully open doors. The objectives of the present study are to perform Large Eddy Simulation (LES) of a large scale fire propagating inside confined and ventilated compartments, and assess the capabilities of the present LES tool applied to a well specified fire scenario. A key part of this assessment is to determine whether FireFOAM can more accurately reproduce the flow variables in comparison to other commercially available fire solvers. FireFOAM utilizes the Eddy Dissipation Concept (EDC) for combustion, discrete ordinate method for radiation, and k equation model for the Sub Grid Scale (SGS) closure. The experimental conditions are reproduced as closely as possible in the simulation. The numerical predictions focus on transient and steady-state temperature, major species concentration, velocity, and pressure in the different rooms. Detailed comparison of the FireFOAM results are made with a Fire Dynamic Simulator (FDS) study and the available experimental data. In general, FireFOAM shows good agreement between the LES results and the experimental data for temperature, velocity, species concentration, and pressure for most compartments. However, in comparison to FDS, FireFOAM over-predicts the fuel consumption rate. The variation in the fuel consumption rate between FireFOAM and FDS is due to the differences in the formulation of the residence time in the EDC combustion model by the two numerical codes.

Acknowledgments

I would like to thank my supervisor, Professor Cécile Devaud for providing assistance and guidance on my research throughout the duration of my MASc studies. Special thanks to Dr. Tarek Beji for providing the FDS results and suggestions. In addition, I would like to thank Professor Beth Weckman for being a great mentor. I would also like to thank my friends and colleagues in the Turbulent Combustion Modeling Group for their valuable support, especially Jeffrey Labahn, Daniele Dovizio, and Seung Hi Lee. Financial support from Canadian Nuclear Safety Commission (CNSC) and University of Waterloo Fire Research Labs are gratefully acknowledged. Also, thanks to Sharcnet and Scinet for providing the computational resources.

Table of Contents

Author's Declaration **ii**

Abstract **iii**

Acknowledgments **iv**

List of Tables **x**

List of Figures **xii**

1 Introduction **1**

1.1 Overview 1

1.2 Objectives 2

1.3 Outline 3

2 Background **5**

2.1 Fire building codes 5

2.2 Fires 6

2.2.1 Nature of fuels 6

2.2.2 Pyrolysis 6

2.2.3 Heat release rate 7

2.2.4 Diffusion flame 7

2.3 Compartment fires 7
2.3.1 Gaseous products of combustion in compartment fires 8
2.3.2 Features of compartment fires 8
2.3.3 Stages of a compartment fire 10
2.3.4 Non-dimensional fire size 11
2.4 Heat transfer modes 12
2.5 Direct numerical simulation 12
2.6 Turbulence modeling 12
2.6.1 Reynolds Average Navier-Stokes (RANS) 13
2.6.2 Large Eddy Simulation (LES) 13
2.7 Mathematical fire modeling 14
2.7.1 Zone models 15
2.7.2 CFD models or field models 15
2.7.3 Limitations of mathematical fire modeling 15
2.8 Combustion modeling with CFD 16
2.8.1 Damköhler number 16
2.8.2 Chemical nature of combustion modeling 17
2.8.3 CFD combustion models 17
2.8.4 Eddy dissipation concept 18
2.8.5 Extension of the EDC model to LES 19
2.9 Fire solvers 20
2.9.1 FireFOAM 20
2.9.2 FDS 21
2.9.3 Key differences between FireFOAM and FDS 21
2.10 Other PRISME numerical studies 21
2.11 Summary 22

3 Model formulation **23**

3.1 Governing equations 23

3.1.1 Conservation of mass 23

3.1.2 Conservation of momentum 23

3.1.3 Energy equation 25

3.1.4 Species transport 26

3.1.5 Equation of state 27

3.1.6 Kinetic energy transport 27

3.2 FireFOAM LES equations 28

3.2.1 Conservation of mass 28

3.2.2 Conversation of momentum 28

3.2.3 Energy transport equation 29

3.2.4 Species transport equation 29

3.2.5 Equation of state 29

3.2.6 Sub grid scale closure 29

3.2.7 Radiation model 30

3.2.8 Combustion model 30

3.3 FDS governing equations 31

3.4 Summary 34

4 Experimental details **35**

4.1 Room layout and configuration 35

4.2 Doorways 37

4.3 Thermal insulation of rooms 37

4.4 Ventilation 38

4.5 Fire source 38

4.6 Ignition system 40

4.7 Material properties 40

4.8 Test schedule . . . 40
4.9 Instrumentation . . . 41
4.10 Summary . . . 41

5 Computational details **42**
5.1 Computational domain . . . 42
5.2 Numerical schemes . . . 44
5.3 Boundary conditions . . . 45
5.3.1 FireFOAM . . . 45
5.3.2 FDS . . . 48
5.4 Summary . . . 49

6 Results **50**
6.1 FireFOAM pre-combustion . . . 50
6.2 Spatial distribution of velocity and temperature . . . 53
6.3 Room 2 - fire room . . . 55
6.3.1 Temperature . . . 55
6.3.2 CO_2 volume fraction . . . 58
6.3.3 Doorway velocity . . . 59
6.3.4 Pressure . . . 65
6.4 Room 1 . . . 66
6.4.1 Temperature . . . 67
6.4.2 CO_2 volume fraction . . . 69
6.5 Room 3 . . . 70
6.5.1 Temperature . . . 71
6.5.2 CO_2 volume fraction . . . 73
6.6 Corridor . . . 74
6.6.1 Temperature . . . 75
6.6.2 CO_2 volume fraction . . . 77
6.7 Summary . . . 78

7 Conclusions **79**

References **81**

List of Tables

4.1 Concrete material properties 40

4.2 Rockwool insulation material properties 40

6.1 Room 2 - temperature comparison between FireFOAM, FDS, and experimental data in the steady-state region. 55

6.2 Room 2 - CO_2 comparison between FireFOAM, FDS, and experimental data in the steady-state region. 58

6.3 Velocity comparison between FireFOAM, FDS, and experimental data in the steady-state region for the doorway between Room 1 and Room 2. . . . 60

6.4 Velocity comparison between FireFOAM, FDS, and experimental data in the steady-state region for the doorway between Room 2 and Room 3. . . . 62

6.5 Velocity comparison between FireFOAM, FDS, and experimental data in the steady-state region for the doorway between Room 2 and the Corridor. 63

6.6 Room 1 - temperature comparison between FireFOAM, FDS, and experimental data in the steady-state region. 67

6.7 Room 1 - CO_2 comparison between FireFOAM, FDS, and experimental data in the steady-state region. 69

6.8 Room 3 - temperature comparison between FireFOAM, FDS, and experimental data in the steady-state region. 71

6.9 Room 3 - CO_2 comparison between FireFOAM, FDS, and experimental data in the steady-state region. 73

6.10 Corridor - temperature comparison between FireFOAM, FDS, and experimental data in the steady-state region. 76

6.11 Corridor - CO_2 comparison between FireFOAM, FDS, and experimental data in the steady-state region. 77

List of Figures

2.1 Fire dynamics within a confined compartment. Reproduced from A. Trouve and Y. Wang, large eddy simulation of compartment fires [1]. 9

4.1 Isometric view of the diva facility showing Room 1, 2, 3, and 4, and the Corridor. Reproduced from L. Gay et al., MAGIC and Code_Saturne developments and simulations for mechanically ventilated compartment fires [2]. 36

4.2 Temperature, species, and velocity sensors. All dimensions in meters. . . . 36

4.3 Thermal protection for Room 2. Reproduced from H. Prétrel and G. Boioli, PRISME Integral programme [3]. 37

4.4 Thermal protection for Room 3. Reproduced from H. Prétrel and G. Boioli, PRISME Integral programme [3]. 38

4.5 Schematic diagram of the facility's ventilation network. Reproduced from H. Prétrel and G. Boioli, PRISME Integral programme [3]. 39

4.6 Fuel pan and ignition source. Reproduced from H. Prétrel and G. Boioli, "PRISME Integral programme" [3]. 39

5.1 Isometric view of the computational domain of the Diva facility. 43

5.2 Isometric view of the PRISME Integral Test 4 meshes. 43

5.3 The geometric domain in FDS. 44

5.4 Isometric view of the computational domain of the Diva facility. 44

5.5 Bird's eye view for the boundaries for the PRISME Integral test #4. 45

5.6 Experimental velocity profile for the inlets and outlet in PRISME Integral Test 4. 47

5.7 Experimental boundary conditions for the fuel surface. 47
5.8 FDS and experimental fuel surface heat release rate. 49

6.1 Pre-combustion transient pressure profiles - FireFoam vs experimental [3]. . 51
6.2 Pre-combustion transient velocity profiles - doorway between Corridor and Room 2 - FireFoam vs experimental [3]. 51
6.3 Pre-combustion transient velocity profiles - doorway between Room 1 and Room 2 - FireFoam vs experimental [3]. 52
6.4 Pre-combustion transient velocity profiles - doorway between Room 2 and Room 3 - FireFoam vs experimental [3]. 52
6.5 FireFOAM temperature contour plane at t=700s across the fuel pan, Room 1 (Right), Room 2 (Center), and Room 3 (Left). Temperatures are in Kelvin. 53
6.6 FDS temperature contour plane at t=700s across the fuel pan, Room 1 (Right), Room 2 (Center), and Room 3 (Left). Temperatures shown in Kelvin. 53
6.7 FireFOAM velocity contour plane at t=700s across the fuel pan, Room 1 (Right), Room 2 (Center), and Room 3 (Left). Velocities are in m/s. . . . 54
6.8 FDS velocity contour plane at t=700s across the fuel pan, Room 1 (Right), Room 2 (Center), and Room 3 (Left). Velocities are in m/s. 54
6.9 PRISME Integral Test 4 - Room 2 location. 55
6.10 Room 2 - transient temperature profiles predicted by FireFoam compared with experimental data [3]. 57
6.11 Room 2 - transient O_2 volume fraction profiles predicted by FireFoam compared with experimental data [3]. 57
6.12 Steady-state temperature in Room 2. 58
6.13 Room 2 - transient CO_2 volume fraction profiles predicted by FireFoam compared with experimental data [3]. 59
6.14 PRISME Integral Test 4 - Room 1 and Room 2 doorway location. 60
6.15 Doorway between Room 1 to Room 2 - transient velocity profiles predicted by FireFoam compared with experimental data [3]. Velocity corresponds to the velocity component normal to the doorway. 61

6.16 PRISME Integral Test 4 - Room 2 and Room 3 doorway location. 61
6.17 Doorway between Room 2 to Room 3 - transient velocity profiles predicted by FireFoam compared with experimental data [3]. 62
6.18 PRISME Integral Test 4 - Corridor and Room 2 Doorway location. 63
6.19 Doorway between Corridor to Room 2 - transient velocity profiles predicted by FireFoam compared with experimental data [3]. 64
6.20 Steady-state velocity profiles for PRISME Integral Test 4. 65
6.21 Room 2 - transient pressure profile predicted by FireFoam compared with experimental data [3]. 66
6.22 PRISME Integral Test 4 - Room 1 location. 67
6.23 Room 1 - transient temperature profiles predicted by FireFoam compared with experimental data [3]. 68
6.24 Steady-state temperature in Room 1. 69
6.25 Room 1 - transient CO_2 volume fraction profiles predicted by FireFoam compared with experimental data [3]. 70
6.26 PRISME Integral Test 4 - Room 3 location. 70
6.27 Room 3 - transient temperature profiles predicted by FireFoam compared with experimental data [3]. 72
6.28 Room 3 - transient O_2 volume fraction profiles predicted by FireFoam compared with experimental data [3]. 72
6.29 Steady-state temperature in Room 3. 73
6.30 Room 3 - transient CO_2 volume fraction profiles predicted by FireFoam compared with experimental data [3]. 74
6.31 PRISME Integral Test 4 - Corridor location. 74
6.32 Corridor - transient temperature profiles predicted by FireFoam compared with experimental data [3]. 75
6.33 Steady-state temperature in the Corridor. 76
6.34 Corridor - transient CO_2 volume fraction profiles predicted by FireFoam compared with experimental data [3]. 77

Chapter 1

Introduction

In this chapter, the introduction, project objectives, and chapter outlines are going to be covered.

1.1 Overview

Within the nuclear industry, fire represents a significant risk with a Core Damage Frequency (CDF) estimated in the order of 10^{-2} per reactor year [4]. Nuclear power plants have implemented state-of-the-art fire detection and suppression systems to meet the fire safety regulation requirements. However, there is a continuous need to assess the suitability of the existing fire safety measures and further minimize the risks of fire propagation within the nuclear facilities due to numerous and complex fire accidents that may occur. Failure to mitigate fire occurrence can potentially lead to damage in the nuclear core, release of radioactivity from the nuclear power plant, or injury to the public. The nuclear industry commonly uses fire modeling to predict the occurrence of these complex accidental fires. Due to an increase in computational power and the development of complex fire models, mathematical fire modeling is becoming more increasingly used. The process of mathematical modeling is complex and interdisciplinary, requiring accurate modeling of fluid mechanics, combustion, turbulence, species, and heat transfer, to adequately model the fire scenario. In order to assess the performance of these mathematical fire models, detailed experimental studies are required, and the flow parameters obtained from these studies can be compared with the mathematical fire modeling results.

As part of the Propagation d'un Incendie pour des Scénarios Multi-locaux Elémentaires (PRISME) fire research program, Institut de Radioprotection et de Sureté Nucléaire (IRSN)

carried out full-scale experimental compartment fire studies [5] that are used as the basis for the assessment of different fire codes [2, 6, 7, 8, 9]. The performance of these fire codes were assessed based on their ability to predict the changes in temperature, pressure fluctuations, smoke propagation, equipment impacts, ventilation effects, and fire suppression interactions. There are up to 1200 instrumentation devices that capture transient flow parameters within the multi-compartment facility, which include thermocouples, pressure sensors, gas analyzer, thermal flow sensors, flow meters, soot analyzers, video cameras, and an electronic balance. The numerical results could then be compared with the experimental data to assess the performance of the mathematical fire model.

Within the past several decades, Computational Fluid Dynamics (CFD) mathematical fire models have garnered attention from the research community due to its inherent benefits. In addition to being relatively fast and inexpensive when compared with experimental studies, CFD models exhibit attractive qualities, such as the capability of modeling the development of a fire within a compartment, complex geometries, flame spread, large geometries, and structure of pool fires [10]. However, CFD modeling of real fires are within the preliminary stages due to numerous assumptions and simplifications [11]. Nevertheless, these assumptions and simplifications are required to make the numerical simulations computationally feasible.

1.2 Objectives

In the present study, FireFOAM [12] is the selected fire model to be assessed. FireFOAM is a fully compressible Large Eddy Simulation (LES) CFD fire code that uses the OpenFOAM platform, which uses the Finite Volume Method (FVM) to discretize the set of governing equations. This code has been developed by FM Global as part of a research program to create a CFD fire model capable of modeling large-scale fires. In addition, FireFOAM has been applied to different fire scenarios with good predictions for temperature and velocity [13, 14, 15]. To the author's best knowledge, no previous study of a representative PRISME compartment fire scenario using FireFoam has been previously conducted.

The objective of the present study is to investigate the predictive capabilities of FireFOAM applied to PRISME Integral Test 4, which is a multi-room compartment fire configuration with fully open doorways between the rooms. The assessment of this model will be made based on the its ability to predict the features of a fire occurrence within the nuclear facility environment, in terms of changes in temperature and pressure within the facility, fire-ventilation interactions, and propagation of smoke through doorways. In particular, this present study will focus on the predictions of temperature, carbon dioxide (CO_2) and

oyxgen (O_2) concentration, compartment pressure, and doorway velocity. Detailed comparison of the FireFOAM results will be made with a Fire Dynamic Simulator (FDS) [16] study and the available experimental data.

1.3 Outline

Relevant background information will be covered in Chapter 2. Beginning with a brief introduction to fire codes, fire definition, and characteristics of compartment fires. Following, fundamental concepts are reviewed, which includes heat transfer modes, turbulence modeling, and fire modeling. Finally, a summary of previous PRISME numerical studies is presented. This summary gives a brief overview of what has been done in the past and serves as a benchmark for the assessment of new PRISME numerical studies.

In Chapter 3, the model formulations for FireFOAM and FDS are going to be summarized. The chapter starts with a summary of the governing equations, including conservation of mass, conservation of momentum, energy transport, species transport, equation of state, and the kinetic energy transport equation. Following, the LES equations for FireFOAM and FDS are formulated using the governing equations. These formulations also include Sub Grid Scale (SGS) closure, LES filter, radiation model, combustion model, and the simple chemistry equation. These equations are embedded within numerical codes and provide the foundation to simulate these fire events.

In Chapter 4, PRISME Integral Test 4 experimental test conditions are described in detail. First, starting with a full description of the geometric layout of the compartment, including the compartment configuration, location and geometry of doorways, and the location of the fire source. Second, the details of the DIVA facility's ventilation network are outlined. These include the location and operating conditions of the inlet, outlet, and safety circuits. Following, the fire source and ignition system details are shown, including the material properties of the fuel, the fuel surface area, and the power of the ignition system. Finally, the locations of the instrumentation devices that were used as part of this experiment are identified.

In Chapter 5, relevant computational details are outlined for both FireFOAM and FDS. In particular, the temporal and spatial numerical schemes, pressure-velocity coupling algorithms, simulation details, operating conditions, computational domains, meshes, and boundary conditions are described.

In Chapter 6, the results obtained from the FireFOAM and FDS numerical studies are analyzed. The numerical codes are assessed based on their ability to predict the temperature, species, doorway velocity, and pressure within the compartment. This is achieved

through direct comparison with the experimental data. Similarities and differences between the numerical studies and experimental data are outlined, and the implications of the results are suggested.

Finally, in Chapter 7, the conclusions of the present study are summarized. A brief summary of the key findings obtained from the results and analysis section are discussed, and recommendations of future work are outlined at the end of this chapter.

Chapter 2

Background

In this Chapter, all relevant background information will be summarized. This includes information on the building codes, fire definition, compartment fires, heat transfer modes, turbulence modeling, fire modeling, combustion modeling, and details on the FireFOAM and FDS numerical codes.

2.1 Fire building codes

Fire building codes for safety evaluation and design of buildings are generally classified as either prescriptive-based or performance-based [17]. Conventionally, most building codes were largely prescriptive-based, in which the specifications are outlined without any details of the intent or motivation for such specifications. In contrast, performance-based building codes are specification driven and involve a detailed process that require the use of tools such as analytical or computational models [18]. Recently, there has been a general shift of interest from prescriptive-based to performance-based codes for fire safety applications [19]. This is due to the advantages of performance-based building codes over prescription-based building codes. Some of the advantages include design flexibility, cost, and quality achieved [18]. Quality is assessed based on the extent by which the design would meet or exceed the intended expectations of the specification. Nowadays, fire simulation tools such as FDS or Consolidated Model of Fire and Smoke Transport (CFAST) [20] are commonly used for specification requirements in performance-based fire building codes.

2.2 Fires

Fires can be classified as either intended or accidental, based on whether the fire event is expected or unexpected. Intended fires are generated to fulfill a purpose or aid in a process. Some examples of intended fires include Bunsen burners, chimney fires, or camp fires. In contrast, accidental fires may cause unintended property damage or can even lead to death. Consequently, the prevention and/or mitigation of accidental fires are of great interest to the fire research community.

In general, the nature of fires (e.g. flame height, oscillation frequency, under-ventilated or over-ventilated, etc.) is quite complex because it is dependent on several different factors. These factors include combustion kinetics, chemistry, ventilation, thermal properties of boundaries, fire load, and the presence of fire detection and suppression systems [21].

2.2.1 Nature of fuels

When sufficiently mixed with an oxidizing agent, all fuels, whether solid, liquid or gas, will flame in the gaseous state [10]. Therefore, solid and liquid fuels must convert to the gaseous state in order to produce flames. With sufficient thermal energy, liquids evaporate to form a gas phase at the fuel surface, whereas solids undergo chemical decomposition or sublimation to generate volatiles of gaseous products.

The temperature at the surface of flaming solid fuels is generally higher than that of liquid fuels because more energy is needed for chemical decomposition or sublimation than for evaporation [10]. Consequently, the difference in the surface temperature of solid and liquid fuels has different implications on its radiation intensity.

2.2.2 Pyrolysis

Under sufficiently elevated temperatures, solid fuels undergo a phenomenon called pyrolysis, which is the breakdown of the solid particles [10]. Pyrolysis is of interest because many of the combustible items that are commonly found in compartment fires undergo this process. In general, chemical decomposition by pyrolysis occurs in the absence of oxygen to produce gaseous combustible products, liquid products, and char.

In terms of computational modeling of pyrolysis, this task is very difficult since it requires accurate predictions of fuel mass transfer, heat transfer, and decomposition reactions [22]. Currently, pyrolysis is an active area of research and these models are limited to relatively simple fuels [23]. Consequently, within the industry, the Heat Release Rate (HRR) is commonly specified as a fuel input instead of utilizing a pyrolysis model.

2.2.3 Heat release rate

The HRR is a common input for fire models that describes the rate in which heat is generated by a fire. HRR can be modeled using the mechanical method, chemical method, or thermal method [24]. The most common approach for determining the HRR is the mechanical method. In this method, experimental testing is conducted to derive transient HRR profiles for a certain fuel [24]. Some experimental test methods include cone calorimetry (e.g. ISO 5660) or oxygen consumption calorimetry (e.g. ASTM E1354). In contrast, the chemical method involves determining the amount of heat output by using chemistry tabulations. This method is much more computationally expensive and is generally used when accurate predictions of combustion products are required.

2.2.4 Diffusion flame

Common to compartment fires, diffusion flames exhibit properties different from those of premixed flames. Unlike premixed flames where the fuel must be gaseous, diffusion flames can have fuels that are solid, liquid, or gaseous. As stated in Section 2.2.1, given sufficient thermal energy, these solid or liquid fuels must undergo gaseous phase change before flaming can occur. In diffusion flames, the fuel and oxidizer are not mixed prior to reaching the flame front; the oxidizer is supplied from the ambient air. Since air entrainment is necessary to maintain steady flow of oxidizer, diffusion flames must entrain air into the flame front. Generally, when compared to premixed flames, diffusion flames burn slower and have a higher tendency to form soot particles [25].

2.3 Compartment fires

Compartment fires occur within a confined compartment, such as a building, home, car, or garage. The fuel sources in these scenarios are generally solid objects (e.g. sofa, tables, chairs), but can sometimes be liquids (e.g. cooking oil) or gases (e.g. gas leaks). These fires typically occur as a result of an accident and may cause damage and/or lead to fatalities. Unlike turbulent jet flames, which exhibit very high velocity, the main source of momentum in compartment fires is buoyancy. Consequently, these flows have low Froude numbers (ratio of inertia forces to gravitational forces) when compared to turbulent jet flames. Furthermore, compartment fires are generally small to medium scale, with characteristic lengths ranging anywhere between a few centimeters to a few meters [1].

During a fire event, thermal gradients exist between the hot fire plume and surrounding

cool ambient air. The thermal gradient causes a density gradient, which induces a buoyant force. The buoyant force induces a draft of fast, upward moving hot gases that originated from the fire plume. As a result, cool air gets entrained into the hot fire plume to replace the missing hot gases. The process of air entrainment cools the fire plume, dilutes the products, and supplies oxidizer necessary to maintain the fire. Consequently, the velocity increases as a function of the height above the fuel source, characterized by a laminar region directly above the fuel surface to a turbulent region[1] some distance above it.

2.3.1 Gaseous products of combustion in compartment fires

Within compartment fires, the chemical nature and amount of gaseous products that a fire would produce is dependent on the fuel type and ventilation conditions. All combustion products can be classified as either asphyxiants or irritants. Asphyxiants are combustion products that can cause death by suffocation when inhaled, displacing the oxygen that your body requires. The most common asphyxiants present in compartment fires are carbon dioxide, carbon monoxide, or hydrogen cyanide [18]. In contrast, irritants are combustion products that cause chemical burns when exposed to sensitive areas of the human body (e.g. skin, nose, throat, eyes, etc.). If irritants are inhaled, they can cause serious damage to the lungs. The most common irritants present in compartment fires are smoke and soot [18].

2.3.2 Features of compartment fires

The following are common features of compartment fires:

1. Accumulation of gas and combustion products - Smoke and combustion products accumulates below the ceiling. This is because the air within the compartment is restricted to a confined space and hot combustion products rises due to buoyancy.

2. Oxygen deprivation - Unlike natural unconfined fires, compartment fires do not have an unlimited supply of oxidizer. Since sufficient oxidizer is required to maintain a flame, oxygen deprivation can potentially lead to flame extinction.

3. Accumulation of unburnt fuel - In the event where the fire is under-ventilated, unburnt fuel is accumulated within the atmosphere of the compartment [10].

[1] Depending on the size of the fire, this turbulent region above the fuel surface may or may not exist [10].

4. Fire suppression system - Fire suppression systems aid in the mitigation or extinguishment of compartment fires.

5. Hot and cold layer stratification - In compartment fires, the density difference between the hot combustion products and cool ambient air cause a distinct hot upper layer and a cool lower layer (as shown in Figure 2.1) [1].

6. Unconventional fuel sources - As opposed to the conventional fuels, such as gasoline, coal, or wood, the fuels in compartment fires can be anything that is found within the compartment, such as tables, chairs, or clothes.

7. Physical barriers - Physical barriers in compartments (e.g. walls, furniture, etc.) influence the fire dynamics. Obstructions can impede the flow of oxidizer and can also deflect flames on impingement.

8. Soot formation - The slower mixing times (longer residence time) promote soot formation [1].

9. Small velocity scales - The velocity scales in compartment fires are relatively small (0.1 cm/s to 10 cm/s) when compared to jet flames or internal combustion engines, where the velocity scales (10 m/s to 100 m/s) are much greater.

10. Flashover - Flashover is characterized by a significant increase in the fire size and rapid fire spread [1]. More details on flashover can be found in Section 2.3.3.

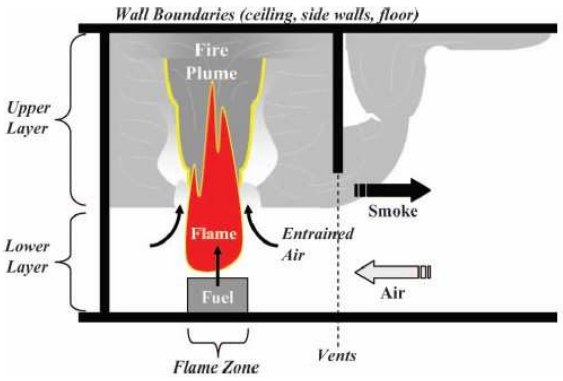

Figure 2.1: Fire dynamics within a confined compartment. Reproduced from A. Trouve and Y. Wang, large eddy simulation of compartment fires [1].

2.3.3 Stages of a compartment fire

There are six distinctive stages in a compartment fire[2], which include ignition, growth or pre-flashover stage, flashover, post-flashover stage, decay stage, and flame extinction [21].

Ignition

Ignition provides the thermal energy required to start the fire. The ignition source can be mechanical, thermal, chemical, or electrical in nature.

Growth or pre-flashover stage

The pre-flashover stage begins after ignition and continues until flashover occurs. Directly following fire initiation, there is an abundance of oxidizer, which allows the fire to burn freely. The flame is localized and the temperature is relatively low, with high temperatures only in regions inside or above the fire plume. The duration of this stage is dependent on the location of the fire source, arrangement and thermal properties of combustible materials, and ventilation conditions.

Flashover

Flashover occurs in the later stages of the fire when the available oxygen within the compartment approaches a critical level. The flashover transition occurs relatively quickly, in comparison to the duration of the growth period. During this stage, most, if not all, combustible fuels within the compartment participate in the fire. Experimentally observed, flashover occurs when the upper layer reaches a threshold temperature of approximately 600°C [18, 26, 27] or when the heat flux at the floor is roughly 20 kW/m^2 [10, 18, 27].

The occurrence of flashover is not guaranteed in all compartment fires but is dependent on the compartment geometry, nature of fuel, arrangement of combustible items in the compartment, degree of radiative and convective heat transfer, and chemistry of the hot gas layer [27].

Due to the complex nature of flashover, current computational modeling of flashover in fire scenarios are not fully representative of the actual physical phenomenon [11].

[2] Following fire initiation, the flame may burn out without ever reaching flashover. This scenario occurs when the fuel is depleted without igniting any other items, there is insufficient ventilation, fire protection equipment is activated, or fire protection personnel intervenes. In this case, the compartment fire would go through less than 6 distinctive stages.

The post-flashover stage

At the start of the post-flashover stage, the fire transitions to fully developed and the flame rapidly spreads to all combustible items within the compartment. Typically, high temperatures of approximately 900 °C to 1100 °C or even higher will be observed [10]. The flame has a tendency to migrate to any oxidizer sources (vents, cracked windows, doorways, etc) and may spread to other compartments, vents, or through cracked windows. In addition, the elevated temperatures typically surpass the threshold of structural members, causing risks of structural damage to load carrying members and potentially leading to structural collapse.

The decay stage

During the decay stage, the fuel becomes depleted and the total heat release rate drops dramatically. This stage is characterized by the continual fall of temperature. Flame extinction is eminent during this stage, although the thermal inertia maintains relatively high temperatures within the compartment for a prolonged period of time.

Flame extinction

Flame extinction occurs when the fire is depleted due to lack of fuel or oxidizer.

2.3.4 Non-dimensional fire size

A non-dimensional fire size governs the flame shape and height in buoyancy-driven fires [28], as shown below

$$Q^* = \frac{\dot{Q}_0}{\rho_\infty T_\infty C_{p,\infty} \left(gD\right)^{1/2} D^2}, \tag{2.1}$$

where Q^* is the non-dimensional fire size, $\dot{Q}_0$ the heat release rate due to combustion, T_∞ the ambient temperature, ρ_∞ the ambient density, $C_{p,\infty}$ the ambient specific heat, g the gravity, and D the characteristic length scale. The flame shape and length change quite dramatically beyond a critical value of Q^* [29]. Once Q^* passes the critical value, the shape changes from a single-flame fire to a multi-flame fire, whereas the flame height changes from scaling linearly with the characteristic length to virtually no correlation with the characteristic length.

2.4 Heat transfer modes

In fires, heat transfer occurs via conduction, convection, and radiation. Conduction heat transfer occurs when heat is transferred through a stationary fluid or solid, induced by thermal gradients. The rate of conduction is related to material properties and thermal gradients across the material. Convection heat transfer occurs by moving liquid or gas, transferring heat from one region to another region. The rate of convection heat transfer depends on the temperature gradient, material properties, and the speed of the moving liquid or gas. Contrary to both conduction and convection, radiation does not require an intervening medium to transfer energy. In radiation, the heat transfer occurs by electromagnetic waves. Radiation occurs when a fluid or solid body exhibits higher temperatures than its environment, causing it to radiate heat to its environment [30]. The rate of radiation heat transfer depends on the temperature difference of the radiating source and its surroundings.

For medium to large scale compartment fires (approximate size of fuel bed > 0.3 m), following fire ignition, convection is the main mode of heat transfer due to the low temperatures in the compartment. As the fire progresses, radiation will eventually become the dominant heat transfer mode. In compartment fires, the three main sources of radiation are hot combustion products, the combustion flame, and hot surfaces such as the ceiling.

2.5 Direct numerical simulation

The most simple and accurate method for numerical modeling of a fluid flow problem is through Direct Numerical Simulation (DNS), where the unsteady, three-dimensional Navier-Stokes equations are solved numerically without simplifications [31]. In terms of numerical accuracy, DNS is superior to turbulence modeling (see Section 2.6) because simplification of the governing equations is not required. However, DNS simulations are only feasible at very low Reynolds numbers (the ratio of inertial forces to viscous forces within a fluid) and small computational domains, because the computational time scales exponentially with the Reynolds number [32].

2.6 Turbulence modeling

Turbulent flows are random, three-dimensional in nature, and time and space dependent [32]. As opposed to laminar flows, turbulent flows occur at higher Reynolds numbers in

which the inertial forces are much greater than viscous forces. Although these flows are random, their statistical properties are predictable and their mean flow quantities are generally reproducible.

Since DNS is very computationally expensive, turbulence modeling provides an attractive alternative for modeling turbulence. However, numerical accuracy is compromised due to the simplifications involved in turbulence modeling. Nevertheless, with the acceptance of a certain amount of numerical uncertainty, turbulence modeling is often used within the industry.

2.6.1 Reynolds Average Navier-Stokes (RANS)

The most popular and widely used turbulence models are based on Reynolds Average Navier-Stokes (RANS) approaches. In RANS models, to represent the mean flow, the instantaneous Navier-Stokes equations are separated into an averaged term and a fluctuating term through Reynolds decomposition. This process results in six additional unknowns called the Reynolds stresses, or categorized as the Reynolds stress tensor [33]. These unknowns are modeled based on the Boussinesq approximation, which relates the Reynolds stresses to the mean velocity gradient and turbulent viscosity. Additional transport equations are required to determine the turbulent viscosity, in order to provide closure to the Navier-Stokes equations.

In terms of drawbacks, these model are known to perform poorly in non-isotropic fields [34] and require model coefficients that vary from configuration to configuration [1]. In comparison to DNS, RANS models are computationally inexpensive but less accurate [33].

2.6.2 Large Eddy Simulation (LES)

In LES, spatial filtering of eddies is employed to separate the large eddies from the small eddies. The large eddies are directly solved without simplifications using the governing equations. Whereas, small eddies are filtered out and represented with a model [35]. This results in a simulation that is relatively accurate and less computationally expensive when compared to DNS.

The process of modeling the small eddies is called Sub-Grid Scale (SGS) modeling. In comparison to larger eddies, smaller eddies take up a large proportion of the computational resources if resolved. In general, small eddies are easier to model accurately than larger eddies because they behave isotropically (at sufficiently high Reynolds numbers). In contrast, large eddies are more difficult to model because they are dependent on domain

configuration, boundary conditions, and body forces [30].

In LES, spatial filtering is done with a filter function $G(x, x', \Delta)$. The spatial filtering is defined as

$$\overline{\phi}(x,t) \equiv \int_{-\infty}^{\infty}\int_{-\infty}^{\infty}\int_{-\infty}^{\infty} G(x,x',\Delta)\,\phi(x',t)\,dx'_1 dx'_2 dx'_3, \tag{2.2}$$

where $\overline{\phi}$ is the filtered function of a flow variable (e.g. pressure, temperature, or species concentration), ϕ is the unfiltered function of a flow variable, and Δ is the cutoff width. For three-dimensional simulations, the cutoff width is

$$\Delta = \sqrt[3]{\Delta x \Delta y \Delta z}, \tag{2.3}$$

where Δx is the length, Δy the width, and Δz the height of a grid cell. Both FireFOAM and FDS use the Top-Hat filter for LES [12], defined as

$$G(x,x',\Delta) = \begin{cases} 1/\Delta^3 & |x-x'| \leq \Delta/2 \\ 0 & |x-x'| > \Delta/2 \end{cases} \tag{2.4}$$

2.7 Mathematical fire modeling

The process of mathematical modeling is an interdisciplinary topic that requires accurate modeling of fluid mechanics, combustion, turbulence, species transport, and heat transfer, in order to adequately reproduce the fire scenario. The integrity of the fire model may be compromised if any of these coupled processes are not properly modeled. However, in most mathematical fire models available within the industry, significant amount of simplifications are employed in order to make the simulations computationally feasible. Therefore, the limitations of the models should be well understood in order to achieve reliable results.

Over the past several decades, the increase in computational power has changed how fire modeling has been conducted. During the early 1980s, mathematical fire modeling was viewed as a research tool and had little to none industrial purposes. However, the advances in mathematical fire modeling techniques and the continual increases in computational power has changed how mathematical fire modeling is viewed [19]. Currently, the two most common types of mathematical fire model are zone models and CFD models.

2.7.1 Zone models

Zone models were developed based upon experimental observations of the smoke stratifications within building fires [11]. The first zone model was initially introduced to solve a single compartment with three distinctive zones, the hot upper smoke layer, the cool lower layer, and the fire plume. Later, it was modified to include the capacity to solve multi-compartment fire scenarios. Simplified conservations equations for energy and mass transport are solved within each zone [26]. Empirical correlations were employed to simplify the equations and reduce the computational cost [10]. The greatest advantages associated with zone models are short computational times and the simplicity of the formulations [36].

2.7.2 CFD models or field models

In CFD modeling of fires, the computational domain is divided into a large number of smaller control volumes and the conservation equations are solved within each control volume for each time step. CFD modeling involves discretization, the transformation of the conservation equations in time and space, to obtain algebraic equations that can be solved within each control volume for each time step [30]. There are several different schemes that can be employed to achieve this, including the finite element, finite difference, or finite volume method. In general, most commercial CFD codes utilizes the finite volume method as its formulation.

In comparison to zone models, these simulations are much more computationally expensive. Despite how computationally expensive they are, there are inherent advantages of CFD models over zones models. Specifically, CFD models generally outperform zone models in its capability of modeling the development of a fire within a compartment, complex geometries, flame spread, large geometries, and structure of pool fires [10]. In addition, unlike with zone models that assume uniform properties within certain zones, CFD models obtain greater resolution of variables of interest (temperature, species, etc.) [26].

2.7.3 Limitations of mathematical fire modeling

As briefly described in Section 2.7, there are limitations associated with mathematical fire modeling imposed by the simplifications involved in its formulation. These simplifications has an effect on the numerical accuracy of the simulations. Some of these limitations include:

1. Common to compartment fires, flame spread is a complex phenomenon that is difficult to model but is apparent in most solid fuel fires. Without a proper flame spread model, it is difficult to determine with great accuracy the probability of flames spreading to other objects within the compartment.

2. Common in most fire simulations, the heat release rate is prescribed instead of modeled. Since the heat release rate is not modeled, the true chemical behavior of the fire is not considered. Even with today's most advanced fire models, chemistry is limited to a few products and few elementary steps are considered.

3. Many combustion models do not consider the chemistry associated with soot, but simply take a yield rate based on experimental studies. Soot is known to have a significant effect on thermal radiation and incorrect modeling of soot would result in poor temperature predictions.

2.8 Combustion modeling with CFD

CFD combustion modeling is a complicated process that requires many simplifications in order to make the solution computationally feasible. The combustion model is used to close the chemical source term in the species transport equation. The choice of combustion model is a vital component in CFD. This is because combustion governs the amount of heat and species release, which has a significant influence on the overall fluid dynamics and heat transfer behavior of the flow. Therefore, understanding the assumptions, simplifications, and concepts behind each combustion model is necessary to determine whether it is applicable to the specific case that one would like to study. Combustion typically involves a large number of species in thousands of chemical reactions that occur simultaneously. In CFD combustion modeling, the number of species and reactions are dramatically reduced (e.g. one-step global chemical equation, two-step global chemical equation, etc) and simplified. Some of the most common CFD combustion models that are used within the industry are shown in Section 2.8.3.

2.8.1 Damköhler number

The Damköhler number (Da) is the ratio of the turbulent (mixing) time scale (τ_t) to the chemical time scale (τ_c). The Damköhler number is

$$D_a = \tau_t/\tau_c, \tag{2.5}$$

The Damköhler number is an important parameter in turbulent combustion modeling because it determines whether the problem is mixing-controlled or chemically-controlled. For a fire scenario, this distinction determines which turbulent combustion model would be applicable. A high Damköhler number ($Da >> 1$) implies that the chemical reaction occurs very quickly and the turbulent mixing is relatively slower; this is therefore a mixing-controlled scenario. In contrast, a low Damköhler number ($Da << 1$) implies that the reaction occurs slowly when compared with the turbulent mixing time; this is chemically-controlled scenario.

2.8.2 Chemical nature of combustion modeling

The process of mathematical modeling of combustion involves modeling the interaction between fuel and oxygen to generate an exothermic reaction that forms products of combustion which exhibit lower bond energy than the reactants [30]. The exothermic reaction releases heat by converting the chemical bond energy into thermal energy. This is a chain reaction process that involves many different elementary reactions. For example, the simplest fuel, methane, involves over 40 different elementary reactions [30]. These elementary steps involve reactive atoms and free radicals (i.e. H ,OH, CH_3) that are created in steps and destroyed in chain termination reactions [10].

2.8.3 CFD combustion models

CFD combustion models are generally separated into different categories based on the key assumptions. Firstly, the infinitely fast chemistry assumption assumes that the chemical reaction happens infinitely fast and once the fuel and oxidizer are sufficiently mixed a reaction will occur. This includes models such as: Bray-Moss-Libby model [37], coherent flame model [38], Eddy Break-Up (EBU) model [39], and Eddy Dissipation Concept (EDC). In contrast, the finite rate chemistry assumption takes into account the reaction rates of the chemical reactions.

Flamelet model
The flamelet model [40] takes into account detailed chemistry and predicts intermediate

and minor species. This model approximates a turbulent flame as a series of stretched laminar flamelets [41]. However, although this model provides detailed chemistry, it is much more computationally expensive when compared with the EDC model.

Presumed Probability Distribution Function (PDF) model
The presumed Probability Distribution Function (PDF) model [42] is a statistical model that determines the unknown variables (e.g. temperature, density, species volume fraction) as a function of a presumed probability distribution function [41]. Although PDF gives reliable predictions for turbulent combustion, solving the PDF at all the cells is computationally expensive compared to EDC [34].

Conditional Moment Closure (CMC) model
Conditional Moment Closure (CMC) [43] uses conditional averages to model the chemical reaction rate. The main idea in CMC is that you can use the fluctuation of a single scalar to represent fluctuations of a turbulent flame [44]. This model is advanced and is capable of modeling soot formation and droplet evaporation/combustion, but is also more computationally expensive than the EDC model.

2.8.4 Eddy dissipation concept

EDC is the chosen combustion model for this numerical study and is used in both FireFOAM and FDS. This model is a turbulent combustion model that uses known parameters to model the chemical reaction rate. This model is commonly applied within the industry and the fire research community due to its simplicity and its applicability to a wide range of fire scenarios. It relates the rate of combustion to the concentration of the limiting species and a characteristic eddy dissipation time.

There are several underlying assumptions within the EDC model. Firstly, this model assumes that chemical reactions only occur within eddies at the Kolmogorov scale [45]. Kinetic energy from the mean flow is transferred to smaller eddies, that is then transferred to even smaller eddies, and further on until it reaches the finest eddies. The finest eddies are expected to have the highest fluctuations (oscillation frequency). These high fluctuations are expected to produce large amounts of viscous stresses that are converted into heat. This assumption is reasonable since upscale transfer and backscatter have negligible effects on the overall fire dynamics of the physical fire scenario [14]. In addition, the EDC model utilizes the infinitely fast chemistry assumption. This assumption drops the detailed chemical kinetics and assumes that reaction rates are solely controlled by the rate of turbulent

mixing [46]. This means that there is a strong dependence on the reliability of the CFD model to capture the turbulence dynamics of the flow, in order to properly predict the mixing dynamics. Also, the EDC model assumes that the fluid in each computational cell is part reacting and part non-reacting [47]. For the reacting part, the residence (mixing) time is expected to be on the same scale as the Kolmogorov time scale [47]. Finally, the EDC model was derived under the assumption of high Reynolds numbers and high Damköhler numbers [48]. Therefore, this model is only applicable to highly turbulent flows.

There are several advantages of utilizing the EDC model for turbulent combustion modeling. Firstly, the EDC model requires no additional transport equations and the mean reaction rate is a function of variables obtained from known quantities. Therefore, this saves computational time since no other coupled transport equations are needed. Based on this premise, the EDC model is less computationally expensive when compared with many other combustion models (PDF, flamelet, etc) [49]. In addition, the concept of EDC is very simple and easy for the user to understand.

In terms of disadvantages, there are several drawbacks of the EDC model. First, chemical reaction rates are nonlinear with respects to temperature and species concentration, so it is difficult to evaluate the mean reaction rates and energy balances [50]. In general, the EDC model has a tendency to over-predict the mean reaction rate, with this effect being most prominent in regions where the flow is highly strained [48]. Second, the EDC model does not account for flame extinction and therefore may have poor predictions during post-flashover [1]. During flashover, the compartment is in the state of oxygen deprivation leading to a higher chance of flame extinction [1]. Third, the EDC constant is configuration dependent and needs to be adjusted accordingly in order to get the reliable predictions. Fourth, in compartment fires, the regions above a fuel source exhibit laminar to transitional zones, but the EDC model was developed for only turbulent regime. Consequently, the EDC model may provide inaccurate predictions for reaction rates and species at this location [49]. Fifth, the EDC model has difficulty handling finite rate chemistry [51]. If detailed chemical species is of interest, this may not be the ideal model. Finally, the EDC model has trouble predicting the combustion characteristics when coupling between multi-step chemistry and turbulence is strong [52].

2.8.5 Extension of the EDC model to LES

For this present study, the EDC model is coupled with LES in both FireFOAM and FDS. Originally, the EDC model was developed for RANS models. However, due to recent interests in LES for turbulent combustion modeling, it has been extended to LES.

When EDC is coupled with the RANS model, the characteristic time is easily obtained

using k and ϵ (e.g. in the $k-\epsilon$ model), but there exist no k and ϵ for the mean flow in LES. k and ϵ only exists in the SGS quantities, therefore approximations must be made in order to adopt the EDC model to LES. For example, as an approximation, Chen et al. [14] notes that other studies have used the sub grid k and ϵ values in the extension to LES. Chen et al. notes that the reaction rate is strongly dependent on grid size for this assumption.

In terms of compatibility with the EDC model, the advantages of using LES over RANS models are:

1. Since larger eddies are resolved instead of being modeled in LES, the flow field and turbulence mixing characteristics are generally more accurately captured than in RANS. This leads to better combustion kinetics predictions because the EDC model relies heavily on accurate modeling of the flow field and turbulent mixing [48].
2. Buckmaster et al. [53] note that because LES takes averages over smaller regions near the flame front, the front instability caused by gas expansion that is evident in RANS models would be better avoided with an LES model.
3. LES outperforms RANS models in highly turbulent flame regions [48]; In RANS models, mean quantities obtained may not be sufficient to describe the instantaneous turbulent effects.
4. LES is better at predicting the unsteady transient phases, large scale flow features, and combustion features that occur in fire simulations [1].

2.9 Fire solvers

For this present study, the differences and similarities between FireFOAM and FDS numerical CFD solvers are outlined.

2.9.1 FireFOAM

FireFoam is a fully compressible fire CFD code that is built on the OpenFoam [54] platform, which uses an LES solver for turbulence modeling. It uses the pressure based solver to solve the Favre-filtered Navier-Stokes equations. For this present study, FireFoam is coupled with the EDC model for combustion, discrete ordinate method for radiation, and the k-equation eddy viscosity model [55] for SGS closure.

2.9.2 FDS

FDS is an numerical LES code that is developed for low-speed, thermally-driven fires. It solves a simplified form of the Navier-Stokes equation suitable for low Mach numbers (< 0.3). For this current study, FDS uses a modified EDC model [16] for combustion, constant yield radiative fraction model for radiation [16], and Deardorff eddy viscosity method [56] for SGS closure.

2.9.3 Key differences between FireFOAM and FDS

FireFOAM and FDS are both LES-based fire CFD solvers that have the capability of utilizing a combination of submodels to model fire scenarios. However, there are key differences between these solvers. FireFOAM's major advantage over FDS is that it is an open-source software. This allows the user full control of modifications of the source codes, to suit their particular needs. In contrast, FDS does not document all of the source codes in the user manuals. By allowing the users to modify the source codes and having full transparency the governing equations and assumptions, FireFOAM poses an attractive alternative to a commercial fire CFD solver like FDS in terms of improved accuracy.

2.10 Other PRISME numerical studies

Several PRISME numerical studies were conducted in the past with varying levels of success. Hosser and Hohm [57] developed a heat transfer model for coupled processes that model the convective heat transfer between gas and solid phases into FDS for PRISME Leak. This model serves as a basis for possible future integration with new pyrolysis models. The results of this study show good agreements between the numerical simulation and experimental data for all the parameters considered. Wahqvist and van Hees [8] had conducted a study using FDS for PRISME Source, PRISME Door, and PRISME Leak tests using a simplified approach for Heating Ventilation and Air Conditioning (HVAC) modeling, based on flow resistance coefficient between nodes and fan curves. Pressure, temperature, and volume flow rates were predicted with reasonable accuracy. However, FDS failed to capture the pressure peaks. Bonte et al. [7] studied a single room in the DIVA facility with a vent and exhaust line using CFAST zone model and Incendie Simulé pour la Sûreté (ISIS) [7] CFD model. For this one compartment scenario, both CFAST and ISIS were able to capture the total relative room pressure, with slightly better predictions with ISIS. For O_2 concentration, only the ISIS CFD model was able to capture these predictions

well. Gay et al. [2] conducted a study using the MAGIC [58] zone model and Code_Saturne [59] CFD code for PRISME Door and PRISME Source tests cases. Good agreement was achieved with MAGIC for the prediction of pressure, doorway velocity, oxygen concentration, vent flow rate, wall heat flux, hot layer temperature, and wall temperature. The authors noted that Code_Saturne was still under development and showed decent results for gas temperature, wall temperature, and O_2 and CO_2 concentration. Pelzer and Klein-Heßling [9] conducted a study using the lumped parameter code COCOSYS [60] on PRISME Source, PRISME Door, PRISME Integral, and PRISME Leak. COCOSYS provided good agreement for the parameters considered (species, pressure, and temperature) with PRISME Source, PRISME Door, and PRISME Leak. However, COCOSYS had difficulties with the predictions of stronger fires, such as with the PRISME Integral. Vaux and Prétrel [6] conducted a study using the SYLVIA zone model [61] on PRISME Source, PRISME Door, and PRISME Leak. SYLVIA appeared to have good predictions of volume flow rate, relative pressure, and density, but had difficulty with the temperature predictions in PRISME Leak and static pressure difference in PRISME Door.

2.11 Summary

In this chapter, all relevant background information was introduced. This included information related to the nature of fires, compartment fires, heat transfer modes, turbulence modeling, fire modeling, combustion modeling, and also a brief summary of the related numerical studies conducted on PRISME cases. The background information leads directly into the topic of the next chapter. Chapter 3 contains the model formulation that is used within FireFOAM and FDS.

Chapter 3

Model formulation

In this Chapter, the governing equations for FireFOAM and FDS are going to be reviewed.

3.1 Governing equations

Firstly, the non-filtered governing equations are introduced. This includes the conservation of mass, conservation of momentum, energy transport, species transport, equation of state, and the kinetic energy transport equation.

3.1.1 Conservation of mass

The governing equation for conservation of mass is

$$\frac{\partial \rho}{\partial t} + \frac{\partial \rho u_j}{\partial x_j} = 0, \tag{3.1}$$

where ρ is the density, t the time, u the velocity, and x the Cartesian coordinate.

3.1.2 Conservation of momentum

The conservation of momentum equations are

$$\frac{\partial \rho u_i}{\partial t} + \frac{\partial \rho u_i u_j}{\partial x_j} + \frac{\partial p}{\partial x_i} = \frac{\partial \sigma_{ij}}{\partial x_j} + \rho g_i, \tag{3.2}$$

where p is the hydrostatic pressure, g_i the gravitational force in the ith direction, and σ_{ij} the stress tensor. The stress tensor, σ_{ij}, is

$$\sigma_{ij} = 2\mu_{eff} S_{ij} - \frac{2}{3}\mu_{eff}\delta_{ij}\frac{\partial u_k}{\partial x_k}, \tag{3.3}$$

where μ_{eff} is the effective dynamic viscosity, S_{ij} the rate-of-strain tensor, and δ_{ij} the Kronecker delta. The effective dynamics viscosity is

$$\mu_{eff} = \rho\nu_{eff}, \tag{3.4}$$

The effective kinematic viscosity is

$$\nu_{eff} = \nu + \nu_t, \tag{3.5}$$

where ν_t is the turbulent kinematic viscosity. The Kronecker delta ,δ_{ij}, is

$$\delta_{ij} = \begin{cases} 1 & i = j \\ 0 & i \neq j \end{cases} \tag{3.6}$$

The components of the rate-of-strain tensor, S_{ij}, is

$$S_{ij} = \frac{1}{2}\left(\frac{\partial u_i}{\partial x_j} + \frac{\partial u_j}{\partial x_i}\right), \tag{3.7}$$

Subbing Eq. 3.4, Eq. 3.5, and Eq. 3.7 into Eq. 3.3, the stress tensor becomes

$$\sigma_{ij} = \rho\left(\nu + \nu_t\right)\left[\left(\frac{\partial u_i}{\partial x_j} + \frac{\partial u_j}{\partial x_i}\right) - \frac{2}{3}\delta_{ij}\frac{\partial u_k}{\partial x_k}\right], \tag{3.8}$$

Subbing Eq. 3.8 into Eq. 3.2, the final form of the conservation of momentum equation is

$$\frac{\partial \rho u_i}{\partial t} + \frac{\partial \rho u_i u_j}{\partial x_j} + \frac{\partial p}{\partial x_i} = \frac{\partial}{\partial x_j}\left[\rho\left(\nu + \nu_t\right)\left(\frac{\partial u_i}{\partial x_j} + \frac{\partial u_j}{\partial x_i} - \frac{2}{3}\delta_{ij}\frac{\partial u_k}{\partial x_k}\right)\right] + \rho g_i, \tag{3.9}$$

3.1.3 Energy equation

The governing equation for energy transport is

$$\frac{\partial \rho h}{\partial t} + \frac{\partial \rho h u_j}{\partial x_j} = \frac{Dp}{Dt} + \frac{\partial}{\partial x_j}\left(q_j\right) - \nabla \cdot \dot{q}_r''' + \dot{q}''', \tag{3.10}$$

where h is the total enthalpy, T the temperature, $\dot{q}_r''$ the radiative heat flux, $\dot{q}'''$ the heat release rate per unit volume from chemical reaction, and q_j the heat flux by thermal conduction. The heat flux by thermal conduction, q_j, is represented by Fourier's law

$$q_j = k_{cond}\frac{\partial T}{\partial x_j}, \tag{3.11}$$

where k_{cond} is the thermal diffusivity. The total enthalpy, h, is

$$h = c_p T, \tag{3.12}$$

where c_p is the heat capacity at constant pressure. Subbing Eq. 3.12 into Eq. 3.11, the heat flux by thermal conduction, q_j, is

$$q_j = \frac{k_{cond}}{c_p}\frac{\partial h}{\partial x_j}, \tag{3.13}$$

The ratio of thermal conductivity to heat capacity is

$$\frac{k_{cond}}{c_p} = \rho D_h + \mu_t, \tag{3.14}$$

where D_h is the thermal laminar diffusion coefficient, μ_t the turbulent dynamic viscosity, and Pr_t the turbulent Prantl number. Subbing Eq. 3.14 into Eq. 3.13 , the heat flux by thermal conduction, q_j, is

$$q_j = (\rho D_h + \mu_t) \frac{\partial h}{\partial x_j}, \tag{3.15}$$

The turbulent dynamic viscosity is

$$\mu_t = \rho \nu_t, \tag{3.16}$$

Subbing Eq. 3.16 into Eq. 3.15, the heat flux by thermal conduction, q_j, is

$$q_j = \rho (D_h + \nu_t) \frac{\partial h}{\partial x_j}, \tag{3.17}$$

Subbing in Eq. 3.17 into Eq. 3.10, the final enthalpy equation is

$$\frac{\partial \rho h}{\partial t} + \frac{\partial \rho h u_j}{\partial x_j} = \frac{Dp}{Dt} + \frac{\partial}{\partial x_j} \left(\rho (D_h + \nu_t) \frac{\partial h}{\partial x_j} \right) - \nabla \cdot \dot{q}''_r + \dot{q}''', \tag{3.18}$$

3.1.4 Species transport

The governing equation for species transport is

$$\frac{\partial (\rho Y_i)}{\partial t} + \frac{\partial (\rho u_j Y_i)}{\partial x_j} = -\frac{\partial (\vec{J_i})}{\partial x_j} + \dot{\omega}_{Y_i}, \tag{3.19}$$

where $\dot{\omega}_{Y_i}$ is the chemical reaction rate, Y_i the species mass fraction, and $\vec{J}_i$ the diffusion flux. The diffusion flux, $\vec{J}_i$, is

$$\vec{J}_i = -\left(\rho D_Y + \frac{\mu_t}{Sc_t}\right)\frac{\partial Y_i}{\partial x_j} = -\rho\left(D_Y + \frac{\nu_t}{Sc_t}\right)\frac{\partial Y_i}{\partial x_j}, \tag{3.20}$$

where D_Y is the species laminar diffusion coefficient and Sc_t the turbulent Schmidt number. Subbing Eq. 3.20 into Eq. 3.19, the final form of the species transport equation is

$$\frac{\partial \rho Y_i}{\partial t} + \frac{\partial \rho u_j Y_i}{\partial x_j} = \frac{\partial}{\partial x_j}\left(\rho\left(D_Y + \frac{\nu_t}{Sc_t}\right)\frac{\partial Y_i}{\partial x_j}\right) + \dot{\omega}_{Y_i}, \tag{3.21}$$

3.1.5 Equation of state

The governing equation for the equation of state is

$$p = \rho R T, \tag{3.22}$$

where R is the ideal gas coefficient.

3.1.6 Kinetic energy transport

SGS modeling is required to account for the sub grid scale turbulence. For this present study, the k equation eddy viscosity model [55] is employed for SGS closure. The kinetic energy transport equation is

$$\frac{\partial \rho k_{SGS}}{\partial t} + \frac{\partial \rho k_{SGS} u_j}{\partial x_j} = \frac{\partial}{\partial x_j}\left(\rho\left(\nu_{eff}\right)\frac{\partial k_{SGS}}{\partial x_j}\right) + \rho P - \rho\epsilon, \tag{3.23}$$

where k_{SGS} is the SGS kinetic energy, P the production of kinetic energy, and ϵ the dissipation of kinetic energy. The effective kinematic viscosity is found 3.5 and the production of kinetic energy is

$$P = -\sigma_{ij}\frac{\partial u_i}{\partial x_j} = \mu\left(\left(\frac{\partial u_i}{\partial x_j} + \frac{\partial u_j}{\partial x_i}\right) - \frac{2}{3}\delta_{ij}\frac{\partial u_k}{\partial x_k}\right)\frac{\partial u_i}{\partial x_j}, \tag{3.24}$$

In addition, the dissipation of kinetic energy is

$$\epsilon = C_\epsilon k_{SGS}^{3/2}\Delta^{-1}, \tag{3.25}$$

and the turbulent kinematic viscosity number is

$$\nu_t = C_k \Delta k_{SGS}^{1/2}, \tag{3.26}$$

where C_ϵ and C_k are model coefficients. For this present study, the default values of the model coefficients were used, which are: $C_k = 0.05$ and $C_\epsilon = 1.048$.

3.2 FireFOAM LES equations

FireFoam uses a spatially filtered, Favre-averaged sets of governing equations for conservation of mass, conservation of momentum, energy transport equation, species transport equation, and radiation model. The proceeding sections summarize the Favre-averaged governing equations that were developed in Section 3.1.

3.2.1 Conservation of mass

The filtered conservation of mass equation is

$$\frac{\partial \overline{\rho}}{\partial t} + \frac{\partial \overline{\rho}\widetilde{u_j}}{\partial x_j} = 0, \tag{3.27}$$

3.2.2 Conversation of momentum

The filtered Navier-Stokes equations are

$$\frac{\partial \overline{\rho}\tilde{u}_i}{\partial t} + \frac{\partial \overline{\rho}\tilde{u}_i\tilde{u}_j}{\partial x_j} = -\frac{\partial \overline{p}}{\partial x_j} + \frac{\partial}{\partial x_j}\left(\overline{\rho}\left(\nu + \nu_t\right)\left(\frac{\partial \tilde{u}_i}{\partial x_j} + \frac{\partial \tilde{u}_j}{\partial x_i} - \frac{2}{3}\frac{\partial \tilde{u}_k}{\partial x_k}\delta_{ij}\right)\right) + \overline{\rho}g_i, \tag{3.28}$$

3.2.3 Energy transport equation

The filtered energy equation is

$$\frac{\partial \overline{\rho}\tilde{h}}{\partial t} + \frac{\partial \overline{\rho}\tilde{u}_j\tilde{h}}{\partial x_j} = \frac{D\overline{p}}{Dt} + \frac{\partial}{\partial x_j}\left(\overline{\rho}\left(D_h + \frac{\nu_t}{Pr_t}\right)\frac{\partial \tilde{h}}{\partial x_j}\right) - \nabla \cdot \dot{q}_r''' + \dot{q}''', \tag{3.29}$$

3.2.4 Species transport equation

The filtered species governing equation is

$$\frac{\partial \overline{\rho}\tilde{Y}_k}{\partial t} + \frac{\partial \overline{\rho}\tilde{u}_j\tilde{Y}_k}{\partial x_j} = \frac{\partial}{\partial x_j}\left(\overline{\rho}\left(D_Y + \frac{\nu_t}{Sc_t}\right)\frac{\partial \tilde{Y}_k}{\partial x_j}\right) + \overline{\dot{\omega}}_{Y_k}, \tag{3.30}$$

3.2.5 Equation of state

The filtered equation of state equation is

$$\overline{p} = \overline{\rho}R\tilde{T}, \tag{3.31}$$

3.2.6 Sub grid scale closure

In LES, eddies with small length scales are spatially filtered out prior to the application of the Navier-Stokes equations, whereas larger eddies are resolved [35]. Smaller eddies are subsequently modeled using SGS modeling. In the current study, the k-equation eddy viscosity model [55] is employed for SGS closure,

$$\frac{\partial \overline{\rho}k_{SGS}}{\partial t} + \frac{\partial \overline{\rho}k_{SGS}\tilde{u}_j}{\partial x_j} = \frac{\partial}{\partial x_j}\left(\overline{\rho}\left(\nu + \nu_t\right)\frac{\partial k_{SGS}}{\partial x_j}\right) + \overline{\rho}\left(\tau_{ij}\frac{\partial \tilde{u}_i}{\partial x_j}\right) - \overline{\rho}\frac{C_\epsilon k_{SGS}^{3/2}}{\Delta}, \tag{3.32}$$

where k_{SGS} is the SGS kinetic energy, P the production of kinetic energy, and ϵ_{SGS} the SGS dissipation of kinetic energy. The turbulent kinematic viscosity number (ν_t) and dissipation of kinetic energy (ϵ_{SGS}) can be found using equations 3.25 and 3.26, respectively.

3.2.7 Radiation model

Radiation is included using the gray mean absorption emission model based on the Finite Volume Discrete Ordinates Method (FVDOM), with the non-scattering medium assumption and spectrally-averaged properties. Generally, the radiative transport equation is expected to be solved over all the spectral bands to achieve reliable radiation estimate. However, this process is very computationally expensive and can be avoided using the mean absorption coefficient approach for species [62]. The mean absorption coefficient depends on the species mass fraction and temperature. The absorption coefficients can be expressed as a temperature dependent polynomial curve fit based on the RADCAL program [63]. The absorption coefficient for each species is found using a polynomial

$$\kappa_i = a_0 + a_1 T + a_2 T^2 + a_3 T^3 + a_4 T^4 + a_5 T^5, \tag{3.33}$$

where a_0, a_1, a_2, a_3, a_4, and a_5 are the model coefficients and κ_i is the absorption coefficient for the i^{th} species.

3.2.8 Combustion model

The EDC model is applied to close the chemical source term in the species transport equation. In EDC, the filtered reaction rate of the fuel is

$$\overline{\dot{\omega}}_F''' = \frac{\bar{\rho} C_{EDC}}{\tau_t} \cdot min\left(\tilde{Y}_F, \frac{\tilde{Y}_{O_2}}{s}\right) = \overline{\rho} C_{EDC} \frac{\epsilon}{k}\, min\left(\tilde{Y}_F, \frac{\tilde{Y}_{O_2}}{s}\right), \tag{3.34}$$

where $\overline{\dot{\omega}}_F'''$ is the fuel reaction rate, τ_t the residence (mixing) time scale, $\tilde{Y}_F$ the fuel mass fraction, $\tilde{Y}_{O_2}$ the oxygen mass fraction, s the stoichiometric oxygen-to-fuel ratio, C_{EDC} the EDC constant, ϵ the turbulent dissipation rate, and k the turbulent kinetic energy. As explained in Section 2.8.5, because there are k and ϵ values for the mean flow, the SGS values for k and ϵ are used as an approximation in the LES extension of the EDC model.

Chemistry

The one-step global reaction is employed for chemistry, which governs the heat release rate and species production/consumption within the fire scenario. This reaction mechanism

assumes that there are no intermediate steps involved and combustion goes from fuel and oxidizer directly to the combustion products in a single step. In reality, there are many intermediate steps and many different combustion products [10]. It is a reasonable approximation if precise predictions of combustion products are not necessary and the primary interest is in the predictions of the mean flow characteristics. Thus, the problem can be simplified and a significant amount computational resources can be saved. The one-step chemistry equation, based on the hydrogenated tetra-propylene ($C_{12}H_{26}$) fuel global chemical balance, that is used in FireFOAM written as

$$C_{12}H_{26} + 18.5\ O_2 + 71.3\ N_2 \rightarrow 12\ CO_2 + 13\ H_2O + 71.3\ N_2, \tag{3.35}$$

3.3 FDS governing equations

FDS uses a spatially filtered, Favre-averaged set of governing equations based on the low Mach number assumption.

Conservation of mass

The filtered conservation of mass equation is

$$\frac{\partial \bar{\rho}}{\partial t} + \frac{\partial \bar{\rho}\tilde{u}_j}{\partial x_j} = 0, \tag{3.36}$$

Conservation of momentum

The filtered conservation of momentum equations are

$$\frac{\partial \bar{\rho}\tilde{u}_i}{\partial t} + \frac{\partial \bar{\rho}\tilde{u}_i\tilde{u}_j}{\partial x_j} = -\frac{\partial \widetilde{(p - p_0)}}{\partial x_i} + \bar{\rho}g - \frac{\partial (\mu_t + \mu)\bar{S}_{ij}}{\partial x_j}, \tag{3.37}$$

where p is the pressure, p_0 the background pressure, μ_t the turbulent dynamic viscosity, and μ the dynamic viscosity.

Species transport

The filtered species transport equation is

$$\frac{\partial \bar{\rho}\tilde{Y}_k}{\partial t} + \frac{\partial \bar{\rho}\tilde{u}_j\tilde{Y}_k}{\partial x_j} = \frac{\partial}{\partial x_j}\left(\bar{\rho}\frac{\nu_t}{Sc_t}\frac{\partial \tilde{Y}_k}{\partial x_i}\right) + \frac{\partial}{\partial x_j}\left(\overline{\rho D_Y \frac{\partial Y_k}{\partial x_j}}\right) + \bar{\dot{\omega}}_k, \tag{3.38}$$

Conservation of energy

The filtered conservation of energy equation is

$$\frac{\partial \bar{\rho}\tilde{h}}{\partial t} + \frac{\partial \bar{\rho}\tilde{u}_j\tilde{h}}{\partial x_j} = \frac{D\bar{p}}{Dt} - \frac{\partial q_j''}{\partial x_j} + \sum_k \frac{\partial}{\partial x_j}\left(\bar{\rho}D_h\tilde{h}_k\frac{\partial \tilde{h}_k}{\partial x_j}\right), \tag{3.39}$$

where h_k is the enthalpy for the kth species.

Combustion model

The EDC model used in FDS is similar to the one used in FireFOAM (Eq. 3.34), except for the formulation of the residence time scale. The residence time is based on the consideration of flow field diffusion, subgrid-scale advection, and buoyancy acceleration [16]. In addition, FDS also notes that the residence time should not be larger than the flame time scale or smaller than the chemical time scale. Consequently, the residence time scale, τ_t, used in FDS is

$$\tau_t = max(\tau_{chem}, min(\tau_d, \tau_u, \tau_g, \tau_{flame}) \tag{3.40}$$

where τ_d is the molecular diffusion time scale, τ_u the turbulent advection time scale, τ_g the buoyancy acceleration time scale, τ_{chem} the chemical time scale, and τ_{flame} the flame time scale. The molecular diffusion time scale is

$$\tau_d = \frac{\Delta^2}{D_F}, \tag{3.41}$$

where D_F is the diffusivity of the fuel species. The turbulent advection time scale is

$$\tau_u = \frac{C_u\Delta}{\sqrt{(2/3)k_{sgs}}}, \tag{3.42}$$

where C_u is the advection time scale constant. FDS uses an advection time scale constant of 0.4. The buoyancy acceleration time scale is

$$\tau_g = \sqrt{2\Delta/g}, \tag{3.43}$$

where g is the acceleration.

SGS closure

FDS uses a variation of the original Deardorff's model[1] that does not solve a transport equation for k_{sgs} [16]. In the Deardorff's model, the equation for μ_t is

$$\mu_t = \rho C_v \Delta \sqrt{k_{sgs}}, \tag{3.44}$$

where C_v is a model constant taken as the default value of 0.1 and k_{sgs} is

$$k_{sgs} = \frac{1}{2}\left(\left(\bar{u} - \hat{\bar{u}}\right) + \left(\bar{v} - \hat{\bar{v}}\right) + \left(\bar{w} - \hat{\bar{w}}\right)\right), \tag{3.45}$$

where $\bar{u}$, $\bar{v}$, and $\bar{w}$ are the cell center average velocity in the x, y, and z direction, respectively. Whereas, $\hat{\bar{u}}$, $\hat{\bar{v}}$, and $\hat{\bar{w}}$ are the weighted average velocity over the adjacent cells in the x, y, and z direction, respectively.

Radiation

In FDS, a radiative fraction model is used for radiation. For this present study, the selected radiative fraction is 35%. Consequently, the solver assumes that 35% of the total energy released from combustion is due to radiation.

Fuel mass flux

For this present study, the HRR is user-specified in FDS. Therefore, the fuel mass flux is calculated to determine the amount of fuel entering the computational domain. The fuel mass flux is determined using the following equation

$$\dot{m}''_f = \frac{f(t)\dot{q}''_{HRR}}{\Delta H_c}, \tag{3.46}$$

where $\dot{m}''_f$ is the mass flux of the fuel, $f(t)$ the user-specified time ramp function, $\dot{q}''_{HRR}$ the user-specified HRR, and ΔH_c the fuel's heat of combustion.

[1] The original Deardorff's model solves a transport equation for k_{sgs}.

Chemistry

Similar to FireFOAM, the one-step chemistry equation is also used in FDS. The simple chemistry equation that is used in FDS is

$$C_{12}H_{26} + 18.5O_2 + 71.3N_2 \rightarrow 12CO_2 + 13H_2O + 71.3N_2 + \nu_{CO}CO + \nu_{Soot}Soot, \quad (3.47)$$

where ν_{CO} is the carbon monoxide yield coefficient and ν_{Soot} the Soot yield coefficient. In this present study, the values of carbon monoxide and soot yield coefficients are selected as 0.012 and 0.042, respectively.

3.4 Summary

In this chapter, the Favre-averaged governing equations for FireFOAM and FDS were introduced. The formulation of the equations were outlined in detail, including the conservation of mass, conservation of momentum, energy equation, species transport, equation of state, kinetic energy transport (SGS closure), LES filter, radiation model, combustion model, and chemistry equation.

Chapter 4

Experimental details

In this chapter, the experimental setup details will be outlined for the PRISME Integral Test 4 experiment. PRISME Integral Test 4 experiment was conducted by IRSN in the Diva research facility (680 m^3) that is located within the JUPITER compartment (3600 m^3). PRISME Integral Test 4 is a multi-room configuration with a turbulent, under-ventilated fire burning Hydrogenated Tetra-Propylene (HTP) and fully open doors between the compartments. Four out of the five compartments within the Diva facility are used in the Integral Test 4 experiment. Consequently, Room 4, located on the second floor, is not used in this series of tests. In addition, the walls of the Diva facility consist of 30 cm thick of reinforced concrete, with Rockwool insulation on some of the walls. The operating pressure within the facility is between -0.1 kPa and 0.3 kPa. All experimental setup details outlined in the present study can also be found in the PRISME Integral programme test report [3].

4.1 Room layout and configuration

For the compartments considered in PRISME Integral Test 4, the room layout and configuration is shown in Fig. 4.2. The enclosure includes Room 1, Room 2, Room 3, and the Corridor. The dimensions of the three rooms are 6 m by 5 m by 4 m high, whereas those of the Corridor are 2.5 m by 15.6 m by 4 m high. Further, the fuel pan, with a surface area of 1 m^2, is located in the center of Room 2 and situated 40 cm above the ground. As shown in Fig. 4.2, the species, velocity, and temperature sensors are mounted at various locations within the compartment.

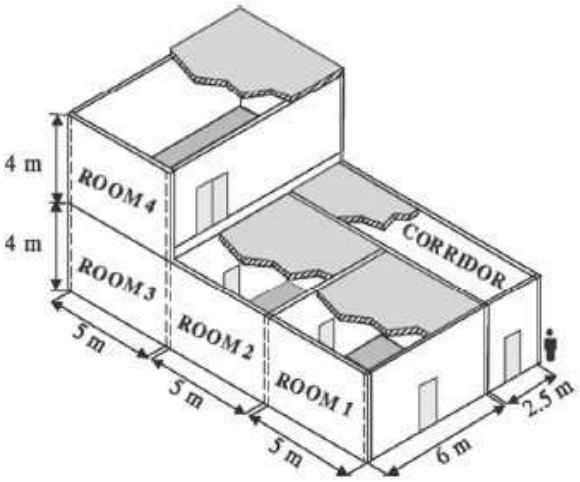

Figure 4.1: Isometric view of the diva facility showing Room 1, 2, 3, and 4, and the Corridor. Reproduced from L. Gay et al., MAGIC and Code_Saturne developments and simulations for mechanically ventilated compartment fires [2].

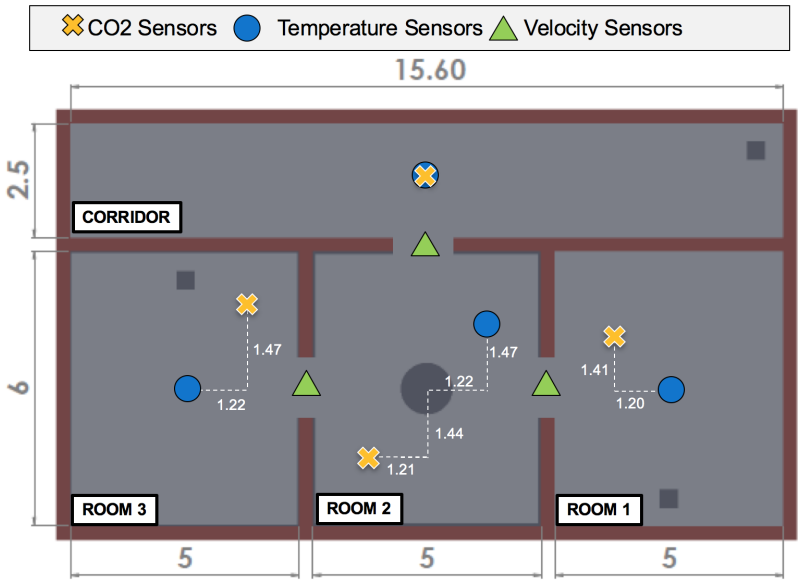

Figure 4.2: Temperature, species, and velocity sensors. All dimensions in meters.

4.2 Doorways

There are three doorways that remained fully opened for the duration of this experiment. This include the doorway between Room 1 and Room 2, the doorway between Room 2 and Room 3, and the doorway between Room 2 and Corridor. The physical dimensions of the doorways are 0.8 m wide by 2.1 m high.

4.3 Thermal insulation of rooms

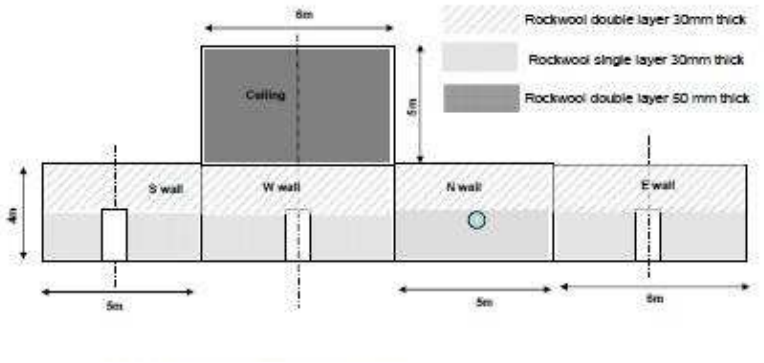

Figure 4.3: Thermal protection for Room 2. Reproduced from H. Prétrel and G. Boioli, PRISME Integral programme [3].

Thermal insulation was placed on some of the walls within the Diva compartment. 50 mm thick Rockwool (Thermipan® 353-750) insulations were used on the ceilings of Room 1, Room 2, Room 3, and the Corridor. For the side walls of Room 2, 60 mm of Rock-wool insulations were placed on the upper half of the walls and 30 mm of Rock-wool insulations were placed on the lower half of the walls. For the side walls of Room 3, 30 mm thick of Rock-wool insulations were placed on all four walls. Finally, Room 1 and the Corridor had no thermal insulation on any of the side walls.

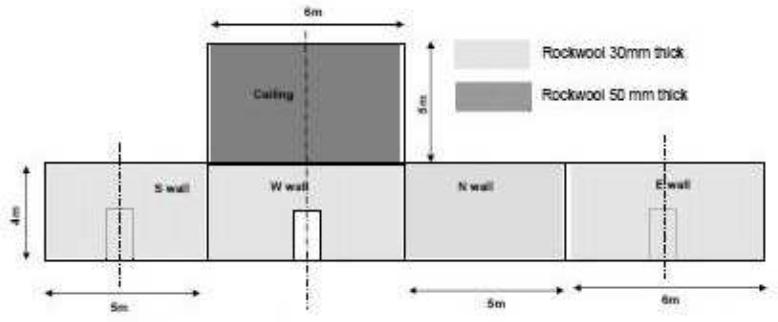

Figure 4.4: Thermal protection for Room 3. Reproduced from H. Prétrel and G. Boioli, PRISME Integral programme [3].

4.4 Ventilation

The Diva facility uses JUPITER's existing ventilation network. As shown in Figure 4.5, there are three circuits within this ventilation network, which includes the inlet (blue), exhaust (green), and safety (red) circuits. The inlet and outlet circuits are both filtered. The rate of airflow can be adjusted within these circuits using valves and dampers and/or with a speed regulator. The safety circuit is connected to Room 1, Room 2, and Room 3 with pressure relief valves set at 0.3 kPa. If the pressure within these rooms exceed the threshold, the safety valves will be activated to relieve the pressure within the compartments. There exists a bypass that allows the operator to decrease the pressure within the compartments before reaching the threshold. This bypass is controlled via an On/Off switch. In addition, a calibrated vacuum relief valve is installed in each compartment and is activated if the pressure within each room drops below -0.09 kPa. For the Integral Test 4, only Room 1 and the Corridor had the inlet circuit vents opened and operating, whereas only Room 3 had the exhaust vent opened and operating.

4.5 Fire source

The fire source consisted of 50 kg of liquid Hydrogenated Tetra-Propylene (HTP) fuel, which was manually poured into the fuel pan. The HTP fuel had a chemical composition of $C_{12}H_{26}$, flash point of 53.5 $°C$, boiling point of 188 °C, and density of 0.758 g/ml (at 20 °C) [3]. The pan is placed on top of 50 mm of Rockwool insulation. The combined pan and insulation rests on top of a weighing system that is used to monitor fuel consumption.

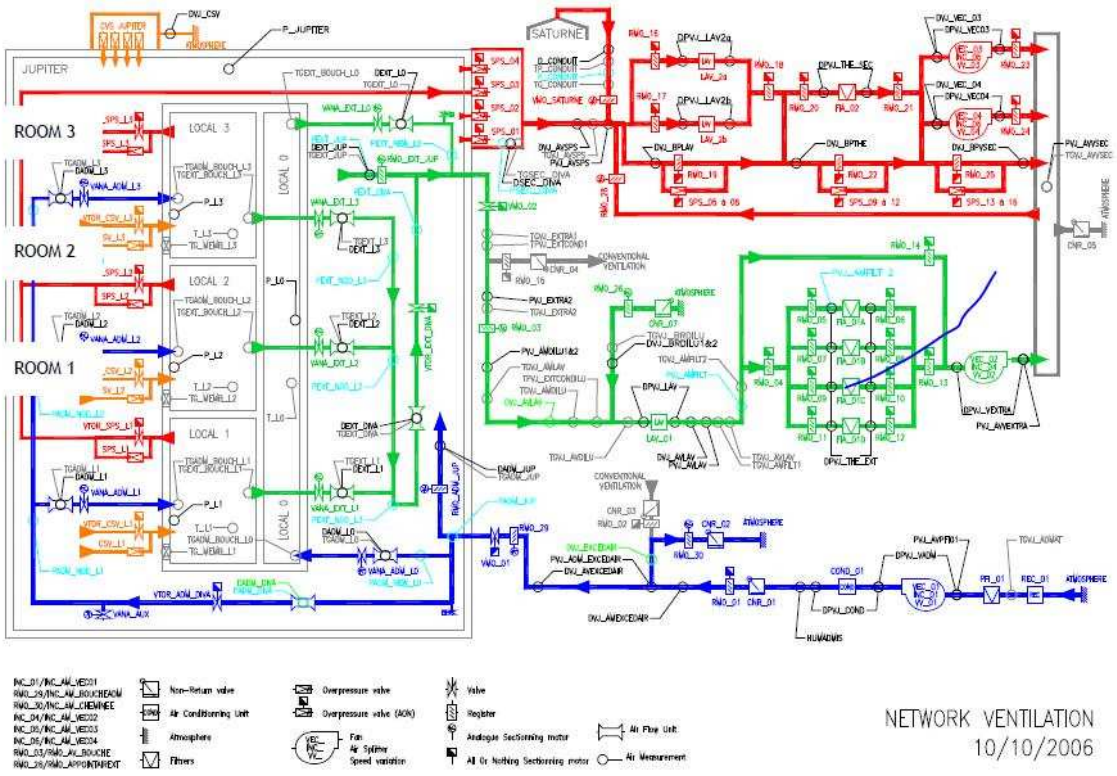

Figure 5 : Schematic diagram of the facility ventilation network.

Figure 4.5: Schematic diagram of the facility's ventilation network. Reproduced from H. Prétrel and G. Boioli, PRISME Integral programme [3].

Figure 4.6: Fuel pan and ignition source. Reproduced from H. Prétrel and G. Boioli, "PRISME Integral programme" [3].

4.6 Ignition system

A gas burner igniter is used to provide the energy, via an electric arc, required to initiate and aid the fuel burning process. This gas burner igniter uses gaseous propane at a flow rate of 5 to 10 liters per minute. The power output of the ignitor is approximately 7.3 to 14.6 kW.

4.7 Material properties

The material properties for concrete and Rockwool insulation are found in Table 4.1 and Table 4.2, respectively.

Table 4.1: Concrete material properties

Concrete	
Conductivity	0.7 W/m K
Specific Heat	0.736 kJ/kg K
Density	2430 kg/m^3

Table 4.2: Rockwool insulation material properties

Insulation	
Conductivity	0.95 W/m K
Specific Heat	0.102 kJ/kg K
Density	0.840 kg/m^3

4.8 Test schedule

The experimental set up for PRISME Integral Test 4 began at 8:30 AM on Thursday June 24th, 2010. At this time, the data acquisition system began recording the variables of interest (pressure, velocity, temperature, species, etc.) within the compartments. The inlet and outlet circuits began running at 10:30 AM on the same day. These circuits ran for approximately 30 minutes until steady state was reached. After steady state has been reached, the Corridor inlet, Room 1 inlet, and Room 3 outlet achieved a mass flow rate

of approximately 500 m^3/h, 2600 m^3/h, and 3100 m^3/h, respectively. Following, at 11:03 AM, the fuel pan was ignited using the igniter. The fire was allowed to burn freely until fire extinction occurred due to fuel depletion. Fire extinction was estimated to occur at 11:29 AM. After flame extinction, the data acquisition system continued to record flow parameters until 11:49 AM. Consequently, the total duration of data acquisition is 69 minutes.

4.9 Instrumentation

There are up to 1200 instrumentation devices that were placed throughout the Diva facility, which includes thermocouples, pressure sensors, gas analyzers, thermal flow sensors, flow meters, soot analyzers, video cameras, and an electronic balance. Thermocouples, gas analyzers, and soot analyzers were arranged vertically in series at different locations within each of the compartments. Similarly, bi-directional velocity probes were placed vertically in series and were mounted at the center of the doorways. In addition, pressure sensors were placed in each of the compartments within the facility.

4.10 Summary

In this chapter, the relevant experimental set up details were introduced. This included the details on PRISME Integral Test 4, the DIVA facility, JUPITER facility, room layout, doorways, thermal insulation, ventilation, fire source, ignition system, test schedule, and instrumentation devices. The experimental data that were collected are used as a basis of comparison for the numerical results.

Chapter 5

Computational details

In this chapter, all relevant computational details will be summarized. This includes the computational domain, meshes, numerical schemes, and the boundary conditions. In the present study, only transient simulations are considered. For each test case, the full simulation (1600 s) is conducted and the results of the final study are analyzed in Chapter 6.

5.1 Computational domain

For FireFOAM, the computational domain consists only of the fluid regions. The walls and insulations are not modeled. Heat transfer through walls is not considered because FireFOAM does not have a conjugate heat transfer model. Some errors are introduced by not considering heat conduction through the walls. However, these errors are expected to be small because the rate of heat conduction is expected to have negligible influence in comparison to the rate of radiation and convection within this physical scenario. A schematic of the computational domain is shown in Figure 5.1.

For this present study, only Cartesian aligned hex meshes are used in FireFOAM. The two meshes considered are 10 cm and 20 cm in length. The 10 cm mesh and 20 cm mesh are shown in Fig. 5.2a and Fig. 5.2b, respectively. The number of cells in the 10 cm and 20 cm meshes are 530,422 and and 86,970, respectively. However, only the results of the 10 cm mesh are shown for brevity.

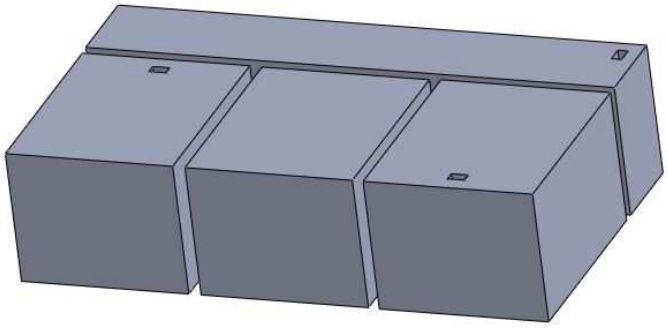

Figure 5.1: Isometric view of the computational domain of the Diva facility.

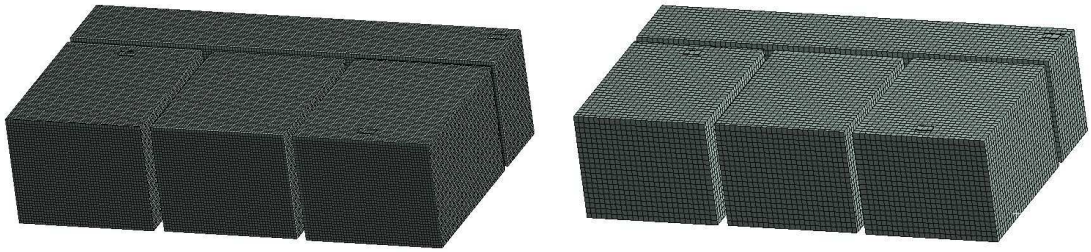

(a) 10 cm mesh. (b) 20 cm mesh.

Figure 5.2: Isometric view of the PRISME Integral Test 4 meshes.

As shown in Fig. 5.3, the FDS computational domain consists of both fluid and solid regions (concrete walls and insulation material). The FDS computational domain is slightly larger than the FireFOAM computational domain. In FDS, an extra 20 cm beyond the exterior walls of the DIVA facility are modeled. Similar to FireFOAM, a Cartesian aligned hex mesh of 10 cm in length spans the entire computation domain. There are 777,600 cells within this mesh. A slice of the x-z plane showing the mesh is shown in Fig. 5.4.

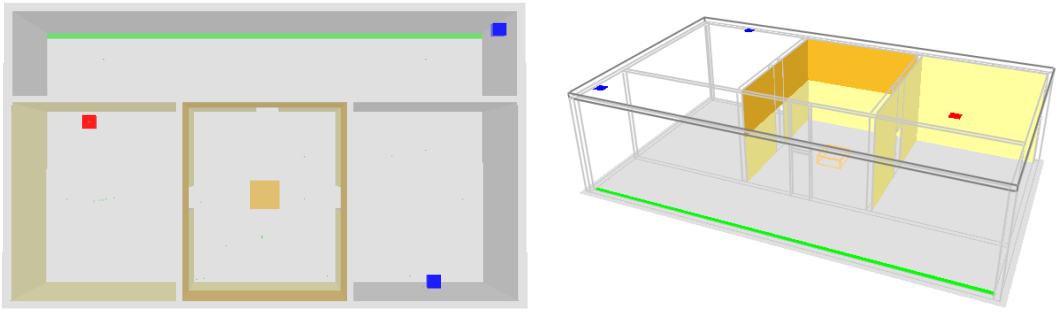

(a) Birds-eye View. (b) Isometric View.

Figure 5.3: The geometric domain in FDS.

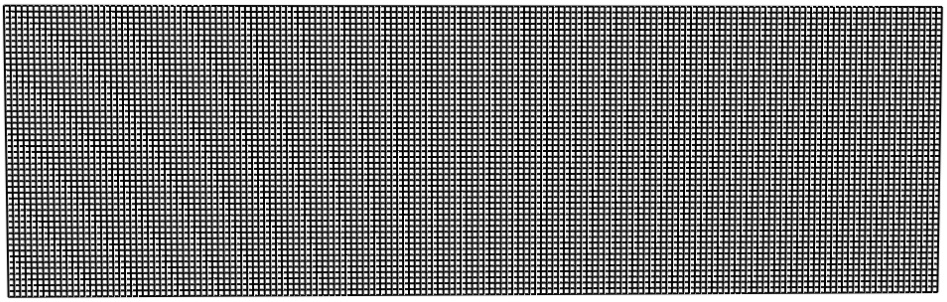

Figure 5.4: Isometric view of the computational domain of the Diva facility.

5.2 Numerical schemes

In FireFOAM, the temporal derivative is discretized using the Euler scheme, whereas the diffusion term and gradient term are discretized using the Gauss linear scheme. The pressure-velocity coupling is done with a combination of PISO and SIMPLE algorithms (PIMPLE). The specific heats for each species are determined using the NASA Polynomial Coefficients [64], the turbulent Prantl number is set at a constant value of 1, and the Courant-Friedrichs-Lewy (CFL) number is limited to 0.4 for all time steps to ensure convergence.

In FDS, the governing equations are discretized using second-order finite differences. Pressure-velocity coupling is done by staggered grid with scalar quantities assigned to the grid centers and velocity at the cell faces. The maximum CFL number is taken as the

default FDS value of 1.0. In addition, the specific heats for each species are determined using NIST-JANAF lookup tables [65].

5.3 Boundary conditions

The boundary conditions for FireFOAM and FDS are summarized in this section.

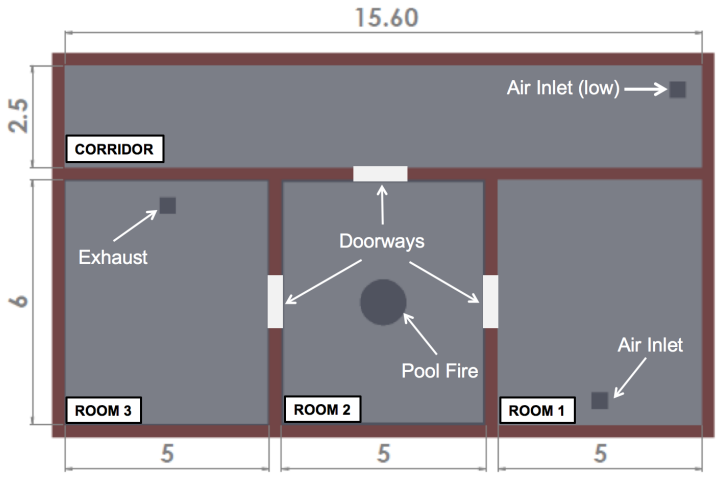

Figure 5.5: Bird's eye view for the boundaries for the PRISME Integral test #4.

5.3.1 FireFOAM

For FireFOAM, boundary conditions are placed on all physical boundaries within the computational domain. A schematic of the DIVA facility outlining the locations of the boundaries are shown in Figure 5.5.

Walls

At the walls, a zero gradient boundary condition is applied for species, temperature, and pressure. These walls are modeled as adiabatic boundaries.

Inlets

For the Corridor and Room 1 inlet boundary conditions, temperature is set at 300 K, O_2 at 20.60 % by volume (22.87 % by mass), Nitrogen (N_2) at 79.40 % by volume (77.13 % by mass), and pressure at 101,036.6 Pa (compartment pressure at $t = 0$). Additionally, different transient velocity profiles are set for the Corridor and Room 1 based on experimental data, as shown in Fig. 5.6a and Fig. 5.6b for the Corridor and Room 1[1], respectively.

Outlet

For the Room 3 outlet, based on experimental data, a transient velocity is set on the outlet boundary, as shown in Fig. 5.6c. The total pressure boundary condition is imposed on this boundary to account for pressure changes as velocity changes. The total pressure equation is written as

$$p_0 = p + 1/2\rho \left|U\right|^2, \tag{5.1}$$

where p_0 is the total pressure, $|U|$ is the velocity magnitude, and p is the pressure.

Fuel surface

For the fire surface, the inlet species is set at 100 % by volume for $C_{12}H_{26}$, pressure at 101,036.6 Pa, and the temperature and velocity are based on experimental data. The fuel mass loss rate and temperature profiles are shown in Fig. 5.7a and Fig. 5.7b, respectively.

[1] As a comparison, the transient FireFOAM velocity output profile is also plotted on each figure to show the differences between the input velocity and what is actually modeled in FireFOAM.

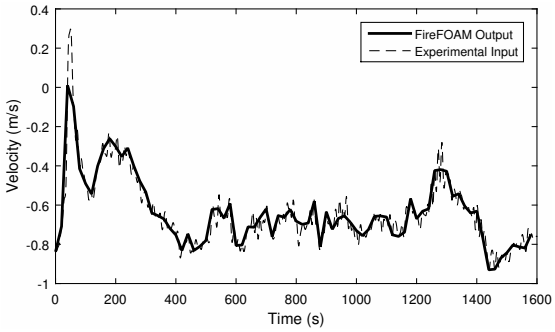

(a) Inlet profile - Corridor.

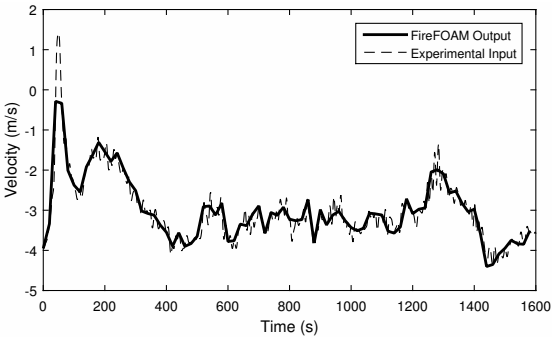

(b) Inlet profile - Room 1.

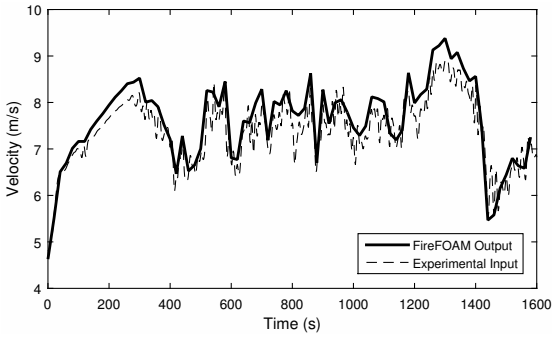

(c) Outlet profile - Room 3.

Figure 5.6: Experimental velocity profile for the inlets and outlet in PRISME Integral Test 4.

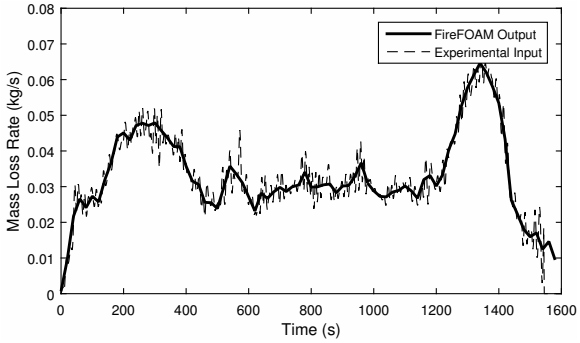

(a) Experimental mass loss rate

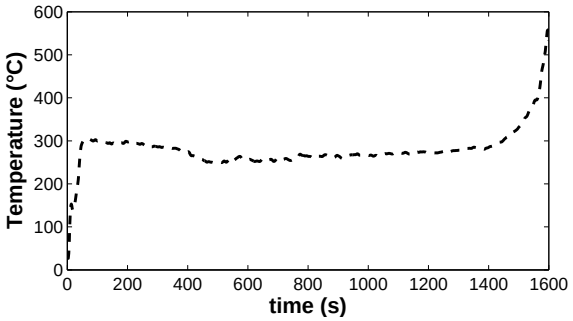

(b) Experimental temperature

Figure 5.7: Experimental boundary conditions for the fuel surface.

5.3.2 FDS

In FDS, boundary conditions are defined for the walls, inlets, outlet, and fuel surface.

Walls

The concrete walls are all set at a constant temperature of 299 K and remained at this temperature for the entire simulation.

Inlets and outlets

The inlets species concentrations are set with the default air composition with 23.054 % O_2 by mass, 76.274 % N_2 by mass, 0.626 % water vapor by mass, and 0.046 % CO_2 by mass. The inlet temperature and pressure are also taken as the default FDS value of 20° C and 101,325 Pa, respectively.

A quadratic fan model is used to model the two inlets and outlet. In this model, the pressure is proportional to the square of the volume flow rate [16]. The mass flow through the vent is dependent on the pressure difference, given by

$$\dot{V}_{fan} = \dot{V}_{max}\ sign(\Delta p_{max} - \Delta p)\sqrt{\frac{|\Delta p - \Delta p_{max}|}{\Delta p_{max}}}, \tag{5.2}$$

where $\dot{V}_{fan}$ is the volume flow rate, $\dot{V}_{max}$ is the maximum flow rate, Δp_{max} is the maximum pressure, and Δp is the pressure difference between upstream and downstream of the vent. Also, duct losses are accounted for by using dimensionless loss coefficients at the inlets and outlets.

Fuel surface

Finally, a heat release rate profile is set on the boundary of the fuel surface. As shown in Fig. 5.8, the heat release rate profile is based on a simplified version of the experimental heat release rate.

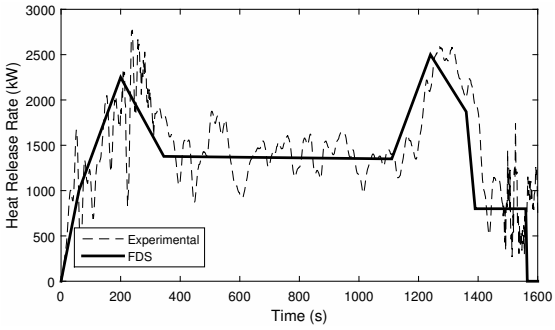

Figure 5.8: FDS and experimental fuel surface heat release rate.

5.4 Summary

In this chapter, all relevant computational details were outlined for both FireFOAM and FDS. This included the numerical schemes, simulation details, computational domain, mesh, and boundary conditions.

Chapter 6

Results

In this section, the results of the FireFOAM simulation will be analyzed and compared to the FDS study and the available experimental data. In particular, the analysis of the predictions of temperature, CO_2 volume fraction, doorway velocity, and compartment pressure will be analyzed.

For the present study, two major species of interest, CO_2 and O_2, are predicted with FireFOAM. The transient numerical CO_2 and O_2 volume fractions follow similar trends, and therefore only the results of CO_2 are shown for brevity.

Similarly, only one out of the four pressure profiles are shown for brevity. This is because the pressure profiles are almost identical from compartment to compartment.

6.1 FireFOAM pre-combustion

The first 100 s of the FireFOAM simulation is run without combustion to match the pre-combustion conditions in the experimento. The results obtained are then compared to the experimental data for the doorway velocity and compartment pressure. The pre-combustion pressure profiles are shown in Fig. 6.1, whereas the pre-combustion velocity profiles for the doorway between the Corridor and Room 2, the doorway between Room 1 and Room 2, and the doorway between Room 2 and Room 3 are shown in Fig. 6.2, Fig. 6.3, and Fig. 6.4, respectively. FireFOAM did a great job with capturing the pre-combustion pressure and velocity. FireFOAM predicts the pre-combustion pressures within 15% of the experimental data and the velocities within 0.3 m/s of the experimental data. These numerical predictions are relatively close to the experimental values and provides a good starting point for the transient simulation.

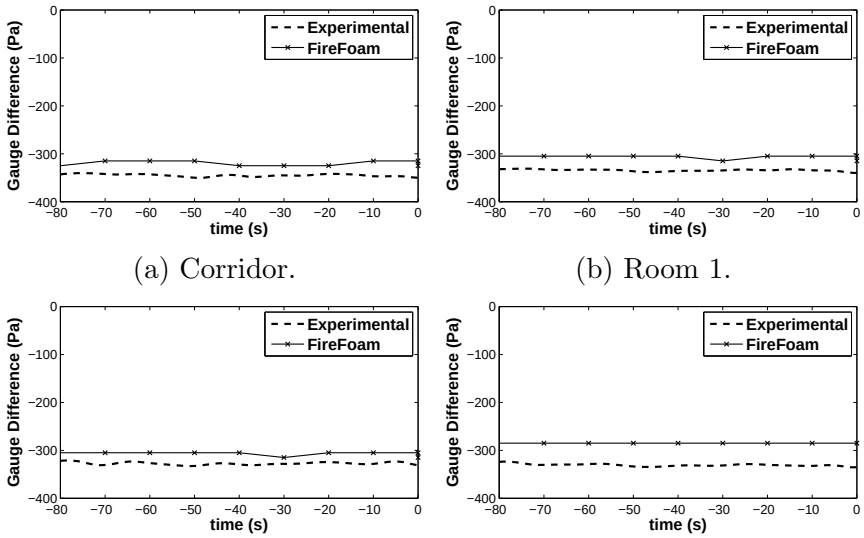

(a) Corridor. (b) Room 1.

(c) Room 2. (d) Room 3.

Figure 6.1: Pre-combustion transient pressure profiles - FireFoam vs experimental [3].

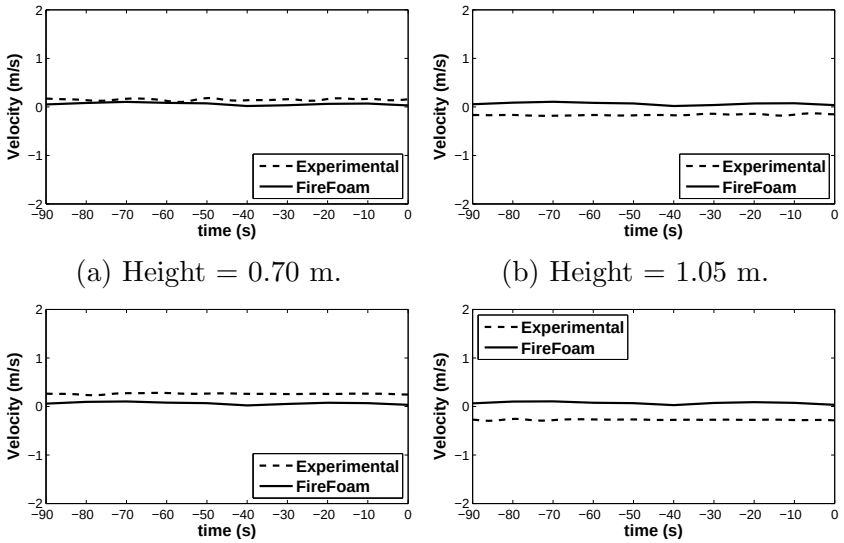

(a) Height = 0.70 m. (b) Height = 1.05 m.

(c) Height = 1.40 m. (d) Height = 1.75 m.

Figure 6.2: Pre-combustion transient velocity profiles - doorway between Corridor and Room 2 - FireFoam vs experimental [3].

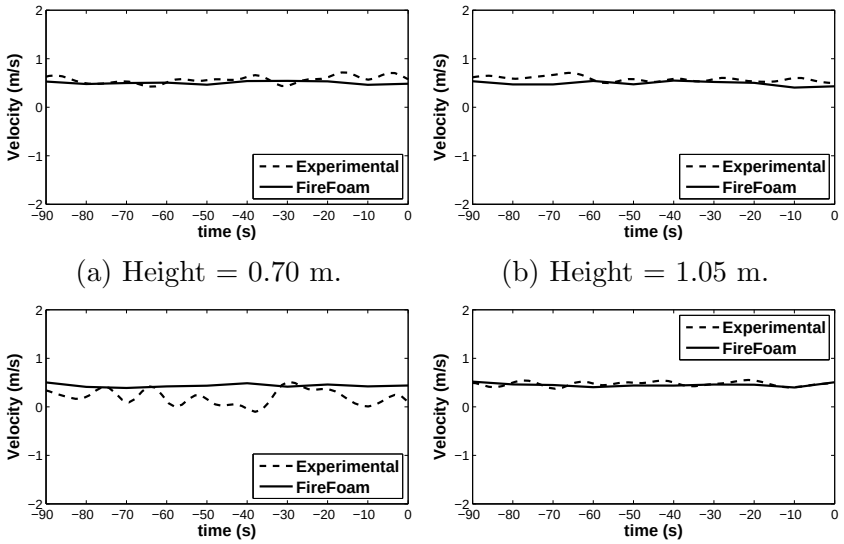

(a) Height = 0.70 m. (b) Height = 1.05 m.

(c) Height = 1.40 m. (d) Height = 1.75 m.

Figure 6.3: Pre-combustion transient velocity profiles - doorway between Room 1 and Room 2 - FireFoam vs experimental [3].

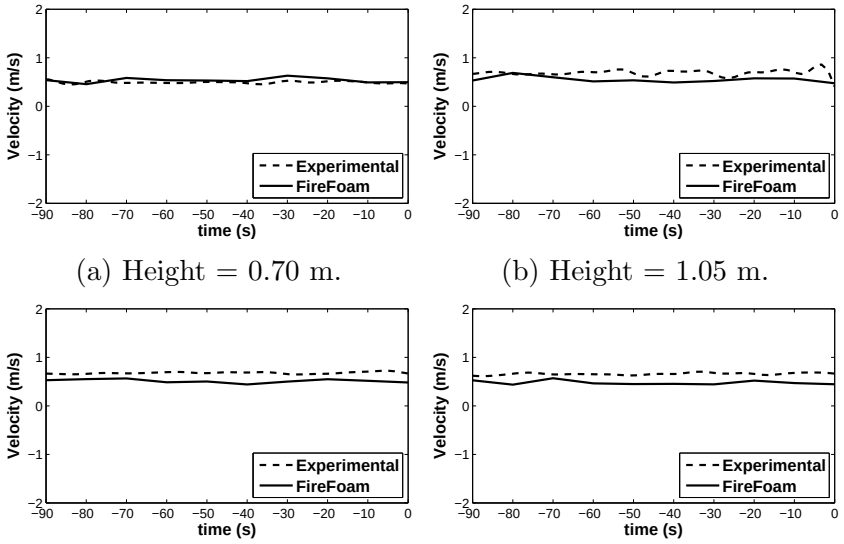

(a) Height = 0.70 m. (b) Height = 1.05 m.

(c) Height = 1.40 m. (d) Height = 1.75 m.

Figure 6.4: Pre-combustion transient velocity profiles - doorway between Room 2 and Room 3 - FireFoam vs experimental [3].

6.2 Spatial distribution of velocity and temperature

For both FireFOAM and FDS, temperature and velocity contours of the x-z plane are plotted to visualize the spatial distribution of the temperature and velocity across the compartments. The y = 6.0 m plane is selected because this plane crosses the fuel surface, the doorway between Room 1 and Room 2, and the doorway between Room 2 and Room 3. Because the steady-state region exists between 400 s and 1200 s, the time of 700 s is taken as a representative of the steady-state region.

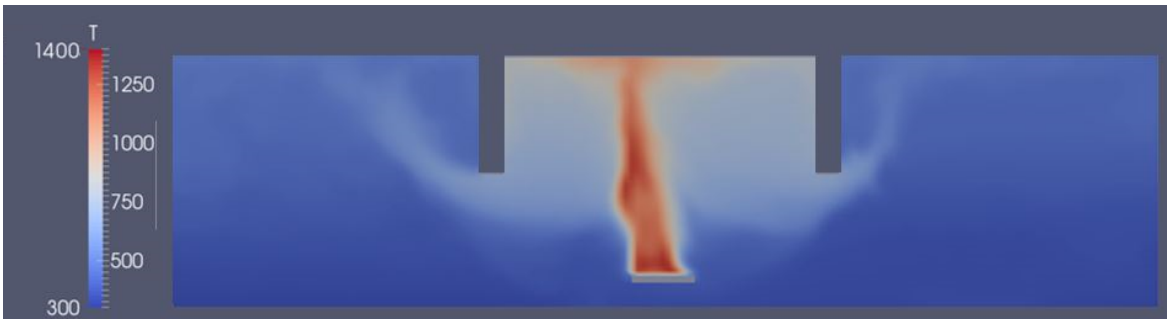

Figure 6.5: FireFOAM temperature contour plane at t=700s across the fuel pan, Room 1 (Right), Room 2 (Center), and Room 3 (Left). Temperatures are in Kelvin.

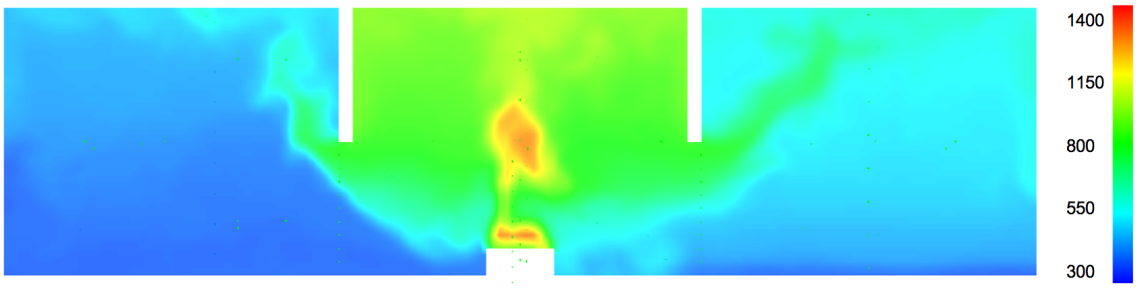

Figure 6.6: FDS temperature contour plane at t=700s across the fuel pan, Room 1 (Right), Room 2 (Center), and Room 3 (Left). Temperatures shown in Kelvin.

The temperature contour is shown in Fig. 6.5 and Fig. 6.6 for FireFOAM and FDS, respectively. FireFOAM and FDS show similar spatial distribution of temperature in Room

1 and Room 3. However, the spatial distribution of temperature above the pool fire in Room 2 is different between FireFOAM and FDS. This can be explained by the difference in the formulation of residence time in the EDC model for the two numerical codes, as described in Section 3.2 and Section 3.3. Different formulations of the residence time leads to different rates in which the fuel is consumed. Faster fuel consumption rates lead to higher temperatures above the fire source. Near the fuel surface, FireFOAM appears to consume fuel at a much faster rate than FDS.

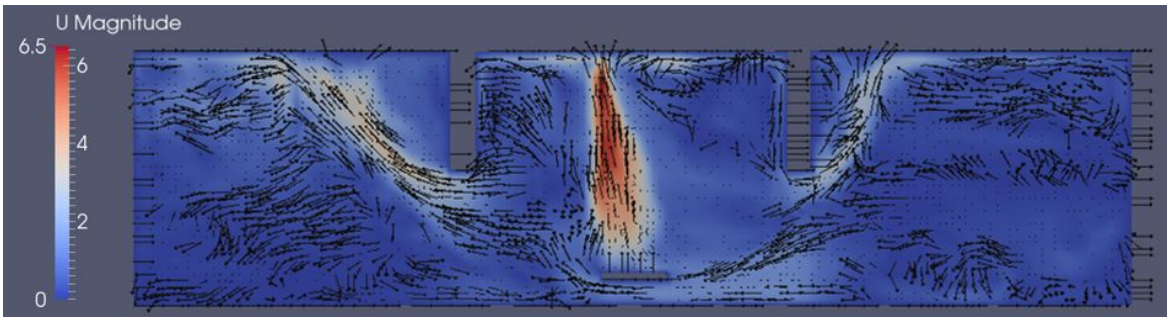

Figure 6.7: FireFOAM velocity contour plane at t=700s across the fuel pan, Room 1 (Right), Room 2 (Center), and Room 3 (Left). Velocities are in m/s.

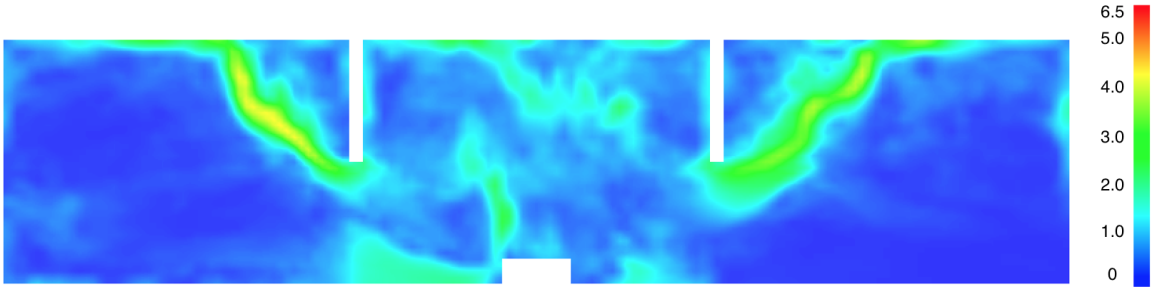

Figure 6.8: FDS velocity contour plane at t=700s across the fuel pan, Room 1 (Right), Room 2 (Center), and Room 3 (Left). Velocities are in m/s.

The spatial distribution of the velocity magnitude is shown in Fig. 6.7 and Fig. 6.8 for FireFOAM and FDS, respectively. In FireFOAM and FDS, as expected, the highest velocity magnitude is seen in the region above the pool fire due to larger temperatures. This region experiences the rapid updraft of buoyant forces due to the temperature gradient between the hot fire plume and cool ambient air. The velocity magnitude in the region

above the fire surface is up to approximately 6.5 m/s for FireFOAM and 4.5 m/s for FDS. For the two doorways considered, there is outflow from Room 2 on the upper region of the doorway and inflow into Room 2 in the lower region of the doorway. This effect is due to the overflow of hot combustion gases that flows out of the fire room through the top portion of the doorway and the replenishment of the cooler air into Room 2 through the bottom of the doorway.

6.3 Room 2 - fire room

In this section, a detailed comparison between the numerical results and experimental data will be conducted for Room 2.

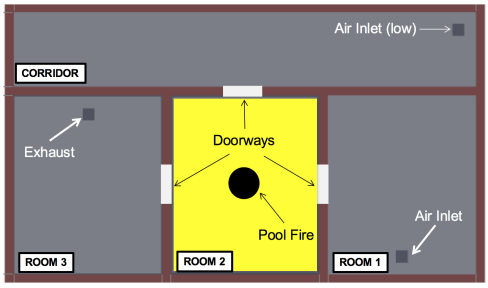

Figure 6.9: PRISME Integral Test 4 - Room 2 location.

6.3.1 Temperature

Table 6.1: Room 2 - temperature comparison between FireFOAM, FDS, and experimental data in the steady-state region.

	Height (m)	**Exp**	**FireFOAM**		**FDS**	
			Temp	**Deviation**	**Temp**	**Deviation**
Room 2	1.05 m	603 K	433 K	28.1 % / 169 K	750 K	24.3 % / 146 K
	2.05 m	834 K	711 K	14.7 % / 122 K	881 K	5.6 % / 47 K
	3.05 m	867 K	738 K	14.8 % / 129 K	938 K	8.1 % / 70 K
	3.90 m	874 K	904 K	3.5 % / 30 K	1024 K	17.1 % / 149 K

The FireFOAM numerical temperature results in Room 2 are good, as shown in Fig. 6.10. The results are compared with the experimental temperature profiles for the sensors located approximately 1.9 m away from the center of the compartment, as shown in Fig. 4.2. Within the steady-state region (500 s to 1200 s), as shown in Table 6.1, the temperature is slightly under-predicted for the three lower sensors. The temperature difference in the steady-state region is approximately 169 K (28.1 %), 122 K (14.7 %), 129 K (14.8 %), and 30 K (3.5 %) for the height of 1.05 m, 2.05 m, 3.05 m, and 3.90 m, respectively. This may be due to combustion modeling errors. The EDC model is known to over-predict the fuel consumption rate near the fuel source, leading to an over-prediction of temperature near the fuel surface and under-prediction of temperature farther away [49]. Because the temperature sensors in Room 2 are located approximately 1.9 m away from the center of the fuel source, the temperatures are expected to be under-predicted at these sensors. Also, the temperature peak occurring at 1350 s is only captured by the lowest height of 1.05 m. The occurrence of this peak is due to oxygen deprivation when the fire transitions from the fuel-controlled to ventilation-controlled scenario, causing an increase in temperature in the regions with low oxygen concentrations. As expected, as shown in Fig. 6.11a, the oxygen concentration is very low at the height of 0.73 m at approximately 1300 s. This explains why the temperature peak is observed at the height of 1.05 m. The opposite trend is observed for the height of 3.90 m because of oxygen depletion. As shown in Fig. 6.11b, oxygen is depleted in Room 2 at 3.2 m. Oxygen depletion causes the temperature to drop dramatically because the required oxidizer to maintain the flame is not present. Consequently, a temperature drop is observed for the height of 3.90 m at 1350 s.

The FDS temperature predictions are marginally better than the FireFOAM temperature predictions for Room 2. FDS predicts the temperature within the initial region (between 0 to 300 s) very well and moderately over-predicts the temperature in the steady-state region for all four heights. Within the steady-state region, the over-predictions of temperature are 146 K (24.3 %), 47 K (5.6 %), 70 K (8.1 %), and 149 K (17.1 %) for the height of 1.05 m, 2.05 m, 3.05 m, and 3.90 m, respectively. The FDS predictions are closer to the experimental data than the FireFOAM predictions for all heights except at 3.90 m. Also, FDS is able to capture the second temperature peak for all heights, whereas FireFOAM only predicts the second temperature peak at 1.05 m. For FDS, the second temperature peak is observed for all heights because oxygen depletion did not occur in the simulation at any of these heights.

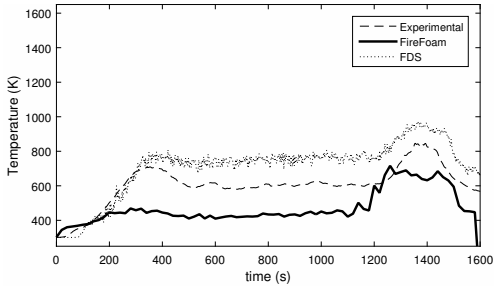

(a) Height = 1.05 m above floor.

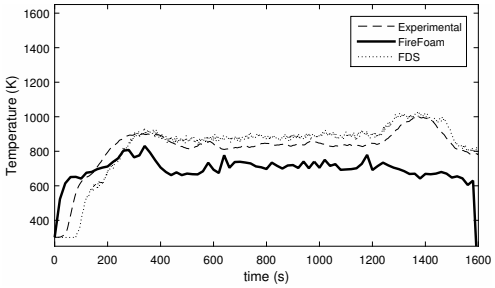

(b) Height = 2.05 m above floor.

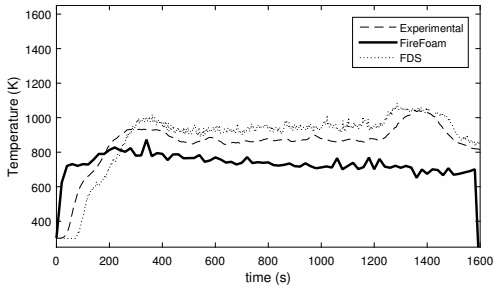

(c) Height = 3.05 m above floor.

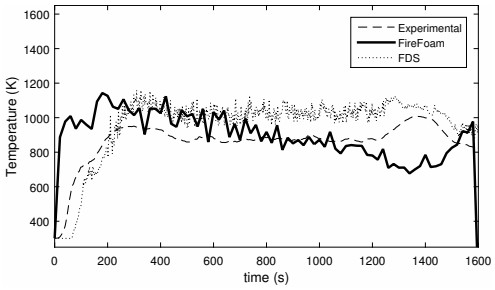

(d) Height = 3.90 m above floor.

Figure 6.10: Room 2 - transient temperature profiles predicted by FireFoam compared with experimental data [3].

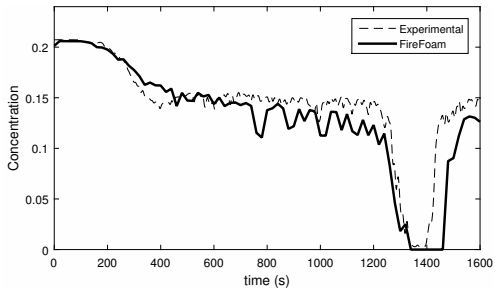

(a) Height = 0.73 m above ground.

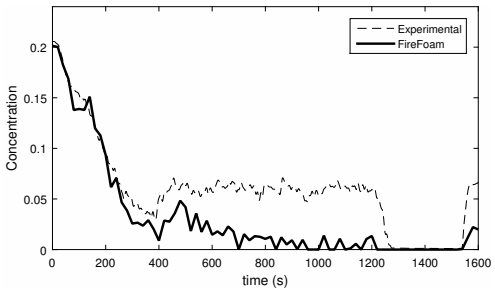

(b) Height = 3.25 m above ground.

Figure 6.11: Room 2 - transient O_2 volume fraction profiles predicted by FireFoam compared with experimental data [3].

In the experimental data and simulation results, there is a prominent steady-state region that exists between 450 s to 1200 s. As a comparison between FireFOAM, FDS, and the experimental data, the steady-state results of temperature are shown in Fig. 6.12 and

Table 6.1. The FireFOAM temperatures are under-predicted and the FDS temperatures are generally over-predicted. The differences in the predictions of the steady-state temperatures between FireFOAM and FDS can be attributed to the differences in residence time modeling between FireFOAM and FDS. For FireFOAM, the residence time scale is based on estimated values of the k and ϵ. In contrast, FDS considers other factors in the residence time. This includes molecular diffusion, turbulent advection, buoyancy acceleration, chemical reaction rate, and flame rate. Any error in estimating the residence time would result in inaccurate fuel consumption rates. By accounting for more than only turbulent mixing, FDS exhibits a steady-state velocity profile that more closely resembles that of the experimental data.

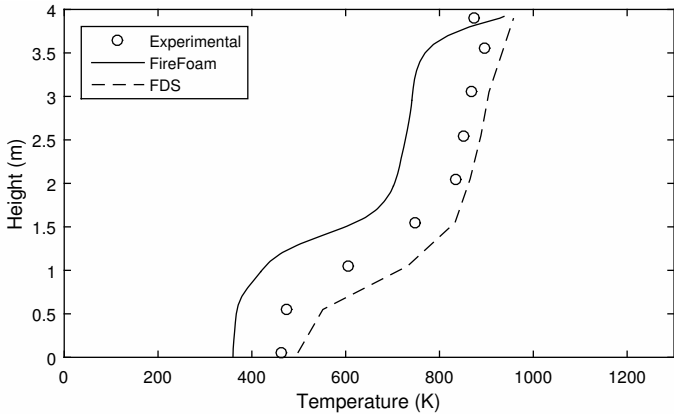

Figure 6.12: Steady-state temperature in Room 2.

6.3.2 CO_2 volume fraction

Table 6.2: Room 2 - CO_2 comparison between FireFOAM, FDS, and experimental data in the steady-state region.

	Height (m)	**Exp**	**FireFOAM**		**FDS**	
			CO_2	**Deviation**	**CO_2**	**Deviation**
Room 2	0.73 m	0.0399	0.0498	24.8 % / 0.0099	0.0526	31.6 % / 0.0126
	3.25 m	0.1013	0.1354	33.6 % / 0.0341	0.093	8.1 % / 0.0082

The FireFOAM transient CO_2 profiles for the heights of 0.73 m and 3.23 m are shown in Fig. 6.13a and Fig. 6.13b, respectively. These sensors are located approximately 1.88 m away from the center of the fuel surface, on the opposite corner of the temperature sensors in this compartment (Fig. 4.2). The CO_2 volume fractions follow closely the experimental data for the lower sensor, and are marginally over-predicted beyond 400 s for the higher sensor. As shown in Table 6.2, the over-prediction is 33.6 % for the higher sensor. The over-prediction of CO_2 volume fraction for the higher sensor is caused by the over-prediction of the fuel consumption near the fuel source. The over-prediction of the fuel consumption rate yields an abundance of the combustion products (e.g CO_2) that accumulate underneath the ceiling of this compartment (fire room).

In contrast, the FDS CO_2 volume fraction profiles are very similar to the experimental data. Aside from the minor over-predictions at the height of 0.73 m between 400 to 1200 s and the minor under-predictions during the initial region (0 to 400 s) for the height of 3.25 m, the FDS CO_2 predictions are great.

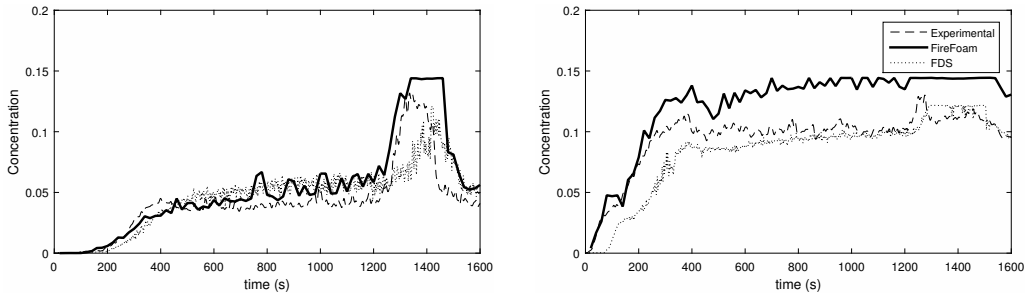

(a) Height = 0.73 m above floor. (b) Height = 3.25 m above floor.

Figure 6.13: Room 2 - transient CO_2 volume fraction profiles predicted by FireFoam compared with experimental data [3].

6.3.3 Doorway velocity

The FireFOAM and FDS transient velocity profiles through the doorway between Room 1 and Room 2, the doorway between Room 2 and Room 3, and the doorway between the Corridor and Room 2 are shown in Fig. 6.15, Fig. 6.17, and Fig. 6.19, respectively. The velocity shown corresponds to a single component parallel to the mean flow direction, consistent with the experimental measurements. The FireFOAM and FDS results are compared with the experimental transient velocity profiles for the sensors located at the center of the doorways, as shown in Fig. 4.2.

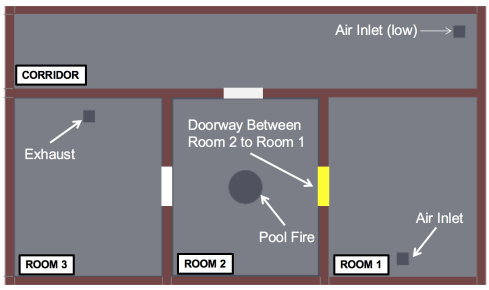

Figure 6.14: PRISME Integral Test 4 - Room 1 and Room 2 doorway location.

Table 6.3: Velocity comparison between FireFOAM, FDS, and experimental data in the steady-state region for the doorway between Room 1 and Room 2.

	Height (m)	**Exp**	**FDS**		**FireFOAM**	
			Velocity	**Deviation**	**Velocity**	**Deviation**
Room 2 to Room 1	0.70 m	1.59 m/s	1.39 m/s	12.8 % / 0.2 m/s	1.15 m/s	27.4 % / 0.43 m/s
	1.05 m	1.56 m/s	0.7 m/s	54.9 % / 0.85 m/s	0.99 m/s	36.5 % / 0.57 m/s
	1.40 m	-1.01 m/s	-1.43 m/s	40.7 % / 0.41 m/s	-0.08 m/s	91.2 % / 0.93 m/s
	1.75 m	-2.09 m/s	-3.05 m/s	45.7 % / 0.95 m/s	-1.46 m/s	30 % / 0.62 m/s

For the doorway between Room 1 and Room 2, as shown in Fig. 6.15 and Table 6.3, FireFOAM and FDS achieve similar results for the heights of 0.7 m, 1.05 m, and 1.75 m, but not at 1.40 m. At 1.40 m, the FDS predictions of velocity are in excellent agreement with experimental values, whereas FireFOAM under-predicts the velocity for the majority of the simulation. FireFOAM under-predicts the velocity magnitude in the steady-state region at 1.40 m by approximately 0.93 m/s. For the other three heights, FireFOAM and FDS both reproduce the velocity well at 0.70 m, slightly under-predict beyond 300 s at 1.05 m, and have deviations of approximately 0.8 m/s in the steady-state region at 1.75 m. Nevertheless, aside from these small deviations, both numerical codes estimate the velocity distribution in this doorway quite well.

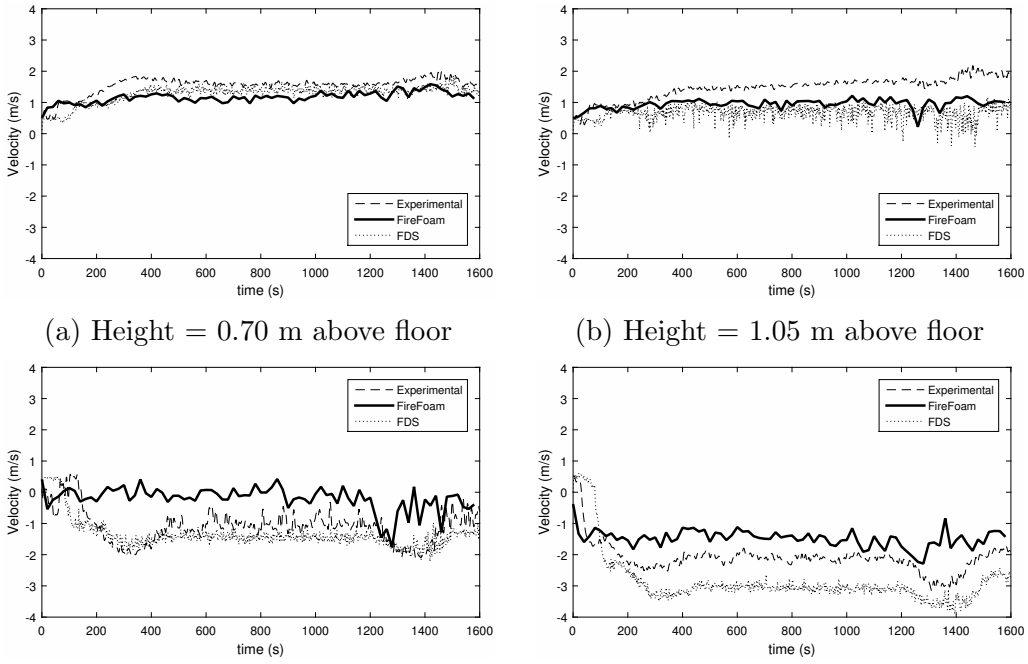

(a) Height = 0.70 m above floor

(b) Height = 1.05 m above floor

(c) Height = 1.40 m above floor

(d) Height = 1.75 m above floor

Figure 6.15: Doorway between Room 1 to Room 2 - transient velocity profiles predicted by FireFoam compared with experimental data [3]. Velocity corresponds to the velocity component normal to the doorway.

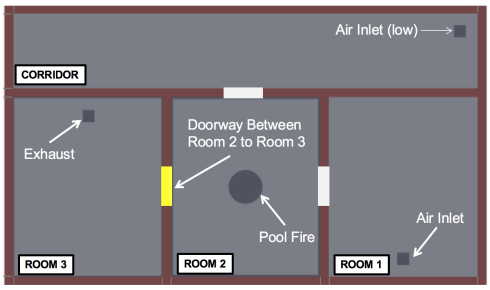

Figure 6.16: PRISME Integral Test 4 - Room 2 and Room 3 doorway location.

The velocity through the doorway between Room 2 and Room 3 is very well predicted by both numerical codes, as shown in Fig. 6.17 and Table 6.4. The FireFOAM and FDS transient velocity profiles follow closely the experimental data at 0.70 m, 1.40 m, and 1.75

m. As for the height of 1.05 m, the FireFOAM and FDS simulations do not exhibit the large velocity fluctuations that are evident in the experimental data. However, the averages of these fluctuations are very close to the profile of the simulation results.

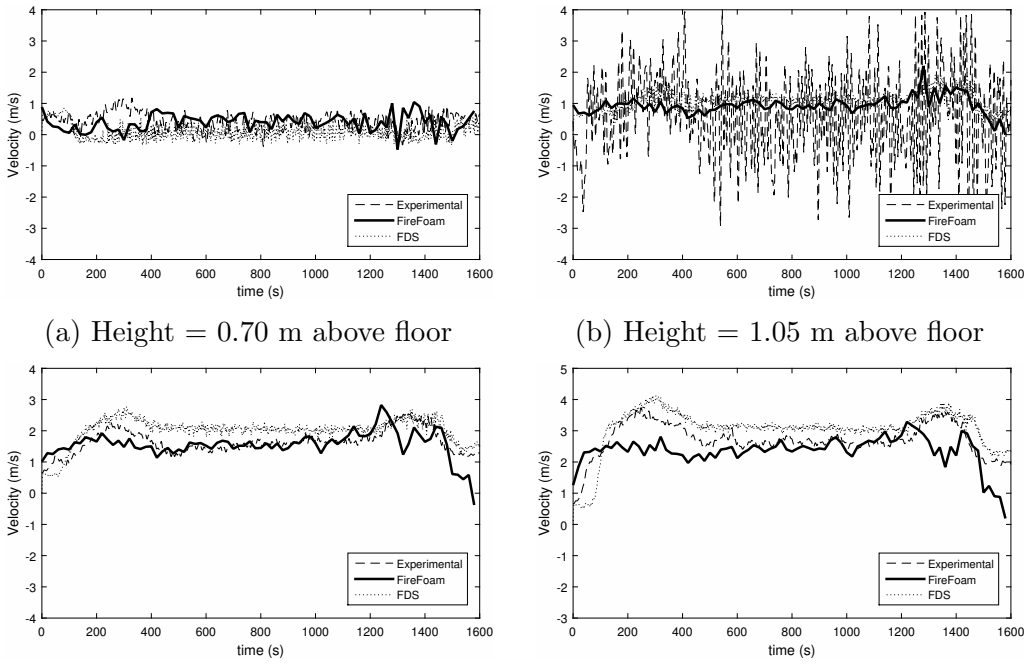

(a) Height = 0.70 m above floor

(b) Height = 1.05 m above floor

(c) Height = 1.40 m above floor

(d) Height = 1.75 m above floor

Figure 6.17: Doorway between Room 2 to Room 3 - transient velocity profiles predicted by FireFoam compared with experimental data [3].

Table 6.4: Velocity comparison between FireFOAM, FDS, and experimental data in the steady-state region for the doorway between Room 2 and Room 3.

	Height (m)	**Exp**	**FDS**		**FireFOAM**	
			Velocity	**Deviation**	**Velocity**	**Deviation**
Room 2 to Room 3	0.70 m	0.36 m/s	0.07 m/s	79.1 % / 0.29 m/s	0.46 m/s	25.7 % / 0.09 m/s
	1.05 m	0.43 m/s	1.11 m/s	155.1 % / 0.67 m/s	0.92 m/s	111.3 % / 0.48 m/s
	1.40 m	1.55 m/s	2.04 m/s	31.7 % / 0.49 m/s	1.58 m/s	1.7 % / 0.02 m/s
	1.75 m	3.09 m/s	2.63 m/s	14.6 % / 0.45 m/s	2.46 m/s	20.2 % / 0.62 m/s

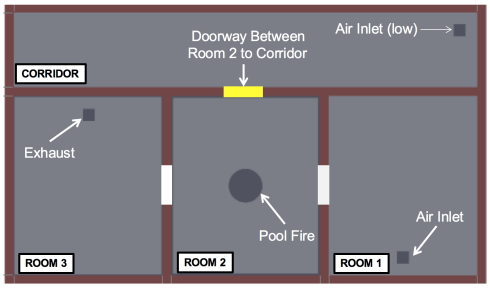

Figure 6.18: PRISME Integral Test 4 - Corridor and Room 2 Doorway location.

Finally, as shown in Fig. 6.19 and Table 6.5, for the doorway between Room 2 and the Corridor, the FireFOAM and FDS transient velocity profiles are well predicted for the two lower locations. At the height of 1.40 m, some irregularities in the experimental doorway velocity data around the 500 s point can be observed. There is a rapid increase in the magnitude of velocity that is only seen for this particular sensor and for that particular time period. It is suspected that there may be some unexpected issues with the experimental apparatus or some events that are not reported in the experiment that resulted in this irregularity, since this effect is only observed for this sensor during this time period. It is also noted that there is no observed steady-state region at the height of 1.40 m. In addition, at the height of 1.75 m, FireFOAM under-predicts the velocity magnitude, while FDS follows the experimental data very closely.

Table 6.5: Velocity comparison between FireFOAM, FDS, and experimental data in the steady-state region for the doorway between Room 2 and the Corridor.

	Height (m)	**Exp**	**FDS**		**FireFOAM**	
			Velocity	**Deviation**	**Velocity**	**Deviation**
Room 2 to Corridor	0.70 m	1.13 m/s	1.08 m/s	4.3 % / 0.04 m/s	0.86 m/s	24.3 % / 0.27 m/s
	1.05 m	0.22 m/s	-0.18 m/s	185 % / 0.40 m/s	0.41 m/s	89.8 % / 0.19 m/s
	1.40 m	-3 m/s	-1.86 m/s	37.8 % / 1.13 m/s	-0.77 m/s	74.3 % / 2.23 m/s
	1.75 m	-2.76 m/s	-3.35m/s	21.4 % / 0.59 m/s	-1.69 m/s	38.5 % / 1.06 m/s

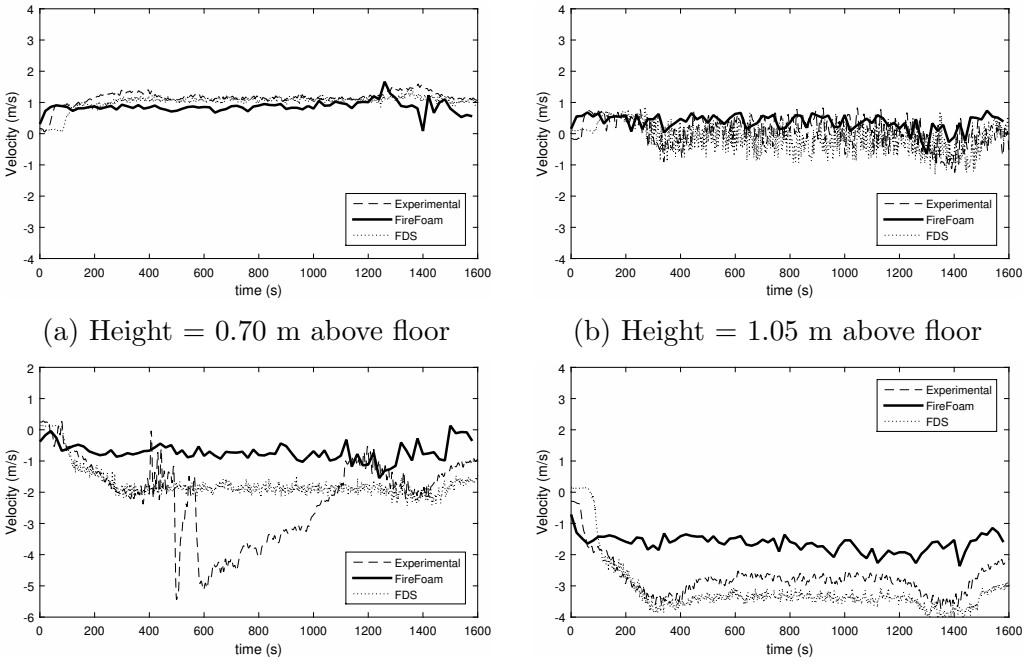

(a) Height = 0.70 m above floor

(b) Height = 1.05 m above floor

(c) Height = 1.40 m above floor

(d) Height = 1.75 m above floor

Figure 6.19: Doorway between Corridor to Room 2 - transient velocity profiles predicted by FireFoam compared with experimental data [3].

As shown in Fig. 6.20, the steady-state velocity profiles of FireFOAM and FDS are good, except for the predictions at one particular point in one of the doorways. In both FireFOAM and FDS, this point is at 1.5 m from the ground in the doorway between the Corridor and Room 2.

Discrepancies observed between the numerical predictions and the experimental data may be due to errors in turbulence modeling and combustion modeling. For turbulence modeling, errors associated with meshing, sub grid-scale modeling, or choice of model (LES) constants would have a direct influence on the overall flow field and will alter the results of the doorway velocity distribution. In addition, chemical kinetics affect the buoyant fire plume temperature and the temperature influences the velocity distribution. As discussed in Section 6.2, FireFOAM appears to slightly over-predict the fuel consumption, leading to errors in the prediction of the flow field.

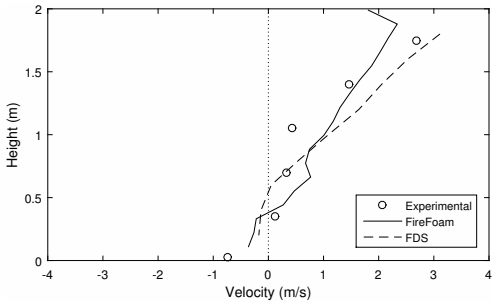

(a) Doorway between Room 2 and Room 3.

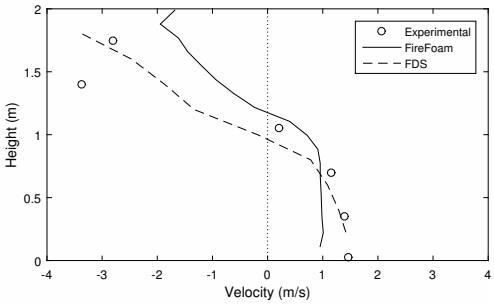

(b) Doorway between Corridor and Room 2

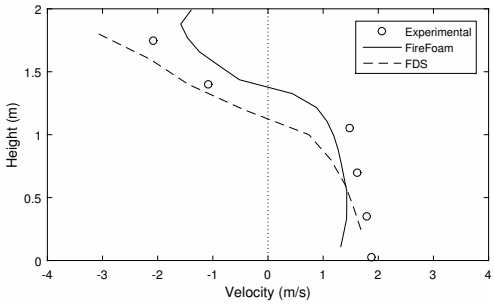

(c) Doorway between Room 1 and Room 2.

Figure 6.20: Steady-state velocity profiles for PRISME Integral Test 4.

6.3.4 Pressure

As shown in Fig. 6.21, the pressure is slightly under-predicted by FireFOAM and slightly over-predicted by FDS within the steady-state region. The pressure remains approximately constant between 200 s and 1200 s at approximately -232 Pa for FireFOAM and 23 Pa for FDS, which are relatively close to the time-averaged pressure of -142 Pa. The pressure fluctuations and pressure peaks seen in the experiments are captured by both FireFOAM and FDS. FireFOAM shows an initial pressure peak of approximately 380 Pa occurring at approximately 20 s and FDS shows an initial temperature peak of 590 Pa occurring at 180 s, whereas the experimental data displays an initial pressure peak of 660 Pa occurring at approximately 50 s. FDS is able to capture the pressure peak occurring at 200 s with slight over-predictions, whereas FireFOAM greatly under-predicts this peak by approximately 300 Pa. The negative pressures in the compartment occurring at approximately 1450 s are not reproduced by FDS but is captured in FireFOAM.

Errors in pressure predictions in FireFOAM may be due to the simplified ventilation network. The physical ventilation network that exists within the experimental facility is quite sophisticated and contains a blowing branch, exhaust branch, and also a safety system, but is modeled as two time-dependent mass flow inlets and one time-dependent mass flow outlet in FireFOAM. For FDS, errors in pressure predictions may be due to fan curve modeling, where the fan curve is determined based on an approximation of the best fit of the experimental data.

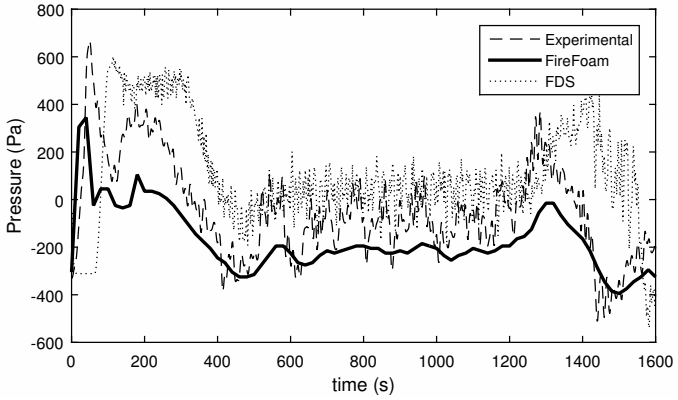

Figure 6.21: Room 2 - transient pressure profile predicted by FireFoam compared with experimental data [3].

6.4 Room 1

In this section, a detailed comparison between the numerical results and experimental data will be conducted for Room 1. This compartment contains the stronger air inlet and therefore has the best ventilation out of the four compartments.

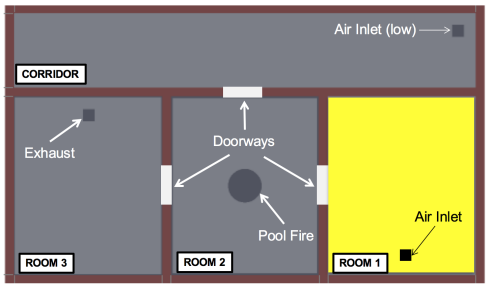

Figure 6.22: PRISME Integral Test 4 - Room 1 location.

6.4.1 Temperature

For FireFOAM, as shown in Fig. 6.23, the agreement between the predicted temperatures and the experimental measurements are excellent in Room 1. FireFOAM estimates the temperature very well at all heights. As shown in Fig. 6.24 and Table 6.6, the steady-state temperature predictions are excellent in this compartment. Other than the marginal over-predictions of temperature observed in two of the sensors (2.05 m and 3.05 m), the FireFOAM results matches the experimental data. Also, the temperature peaks occurring at 350 s and 1400 s are both captured and their magnitudes are greatly predicted.

Table 6.6: Room 1 - temperature comparison between FireFOAM, FDS, and experimental data in the steady-state region.

	Height (m)	**Exp**	**FireFOAM**		**FDS**	
			Temp	**Deviation**	**Temp**	**Deviation**
Room 1	1.05 m	384 K	353 K	7.9 % / 30 K	407 K	6 % / 23 K
	2.05 m	399 K	394 K	1.2 % / 4 K	421 K	5.7 % / 22 K
	3.05 m	438 K	443 K	1 % / 4 K	405 K	7.6 % / 33 K
	3.90 m	509 K	495 K	2.8 % / 14 K	334 K	34.3 % / 174 K

For FDS, similar to FireFOAM, the temperature predictions in Room 1 exceptional for the heights of 1.05 m, 2.05 m, and 3.05 m. The initial region, steady-state region, and the temperature peak occurring at 1350 s are all well captured. However, FDS differs from FireFOAM at the height of 3.90 m, where the temperature is severely under-predicted for the entire test duration. At 3.90 m, the temperature in the initial (0 s to 400 s) and steady-state region (400 s to 1200 s) are under-predicted by up to 300 K.

In general, FDS is comparable to FireFOAM for the height of 1.05 m, 2.05m, and 3.05 m, but FireFOAM appears to be better at the prediction at the height of 3.90 m. This trend is reflected in the steady-state temperature profiles, as shown in Fig. 6.24 and Table 6.6. The FireFOAM predictions are good for the entire test duration, whereas FDS has trouble with the predictions of temperature beyond 2.5 m. Beyond 2.5 m, FDS has significant under-predictions of temperature, by up to 180 K.

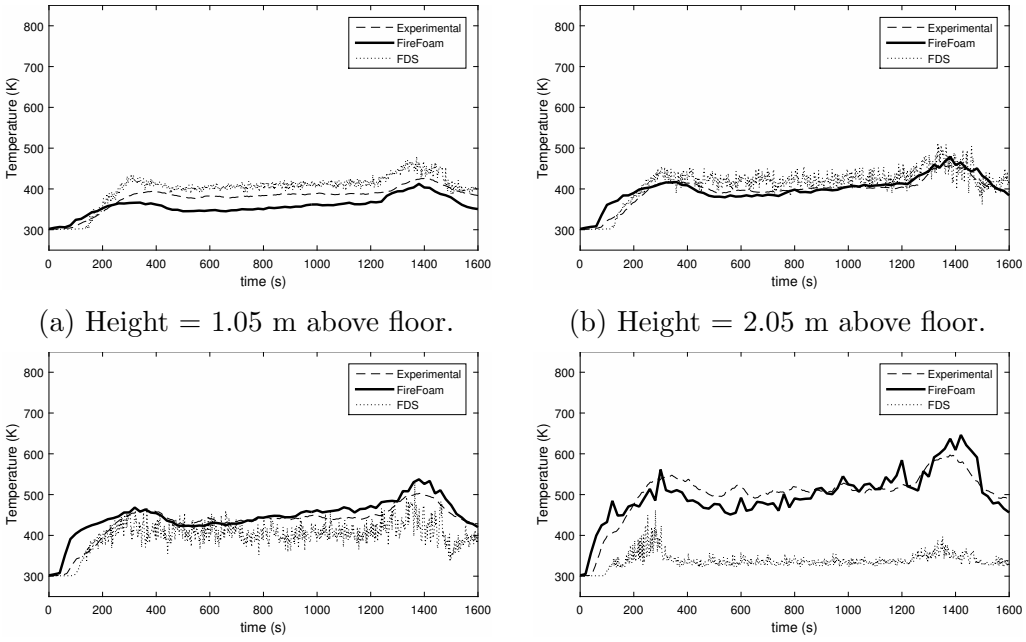

(a) Height = 1.05 m above floor.

(b) Height = 2.05 m above floor.

(c) Height = 3.05 m above floor.

(d) Height = 3.90 m above floor.

Figure 6.23: Room 1 - transient temperature profiles predicted by FireFoam compared with experimental data [3].

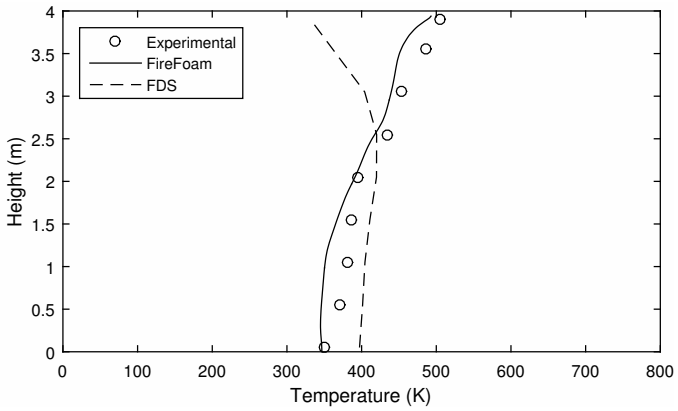

Figure 6.24: Steady-state temperature in Room 1.

6.4.2 CO_2 volume fraction

Table 6.7: Room 1 - CO_2 comparison between FireFOAM, FDS, and experimental data in the steady-state region.

	Height (m)	**Exp**	**FireFOAM**		**FDS**	
			CO_2	**Deviation**	**CO_2**	**Deviation**
Room 1	0.89 m	0.0331	0.0407	23 % / 0.0076	0.0364	10.1 % / 0.0033
	3.23 m	0.0533	0.0546	2.5 % / 0.0013	0.0545	2.2 % / 0.0012

For FireFOAM, the volume fractions are also estimated accurately in this compartment, as shown in Fig. 6.25. The steady-state CO_2 volume fraction concentration predictions are excellent at both heights, with minor over-predictions of 0.0076 (23.0 %) and 0.0013 (2.5 %) for the height of 0.89 m and 3.23 m, respectively. Additionally, there are minor over-predictions of the CO_2 peak occurring at 1350 s. Other than these small discrepancies, the CO_2 volume fractions are very well predicted in this compartment by FireFOAM.

The FDS transient CO_2 volume fraction profiles are in even better agreement with the experimental data. With the exception of small under-predictions during the initial region (between 0 to 400 s), the profiles follow very closely the experimental data for all other regions.

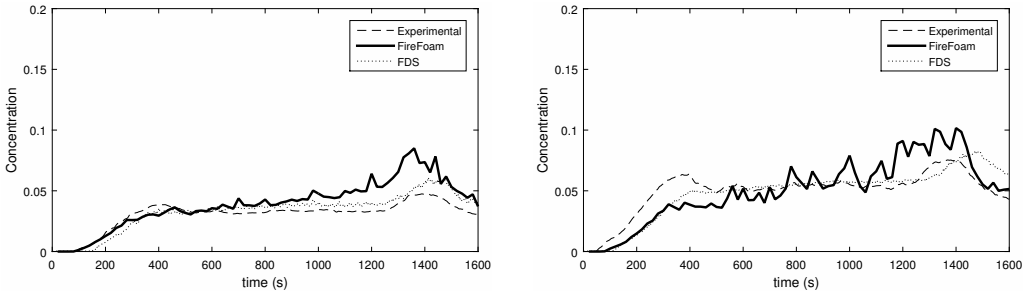

(a) Height = 0.89 m above floor. (b) Height = 3.23 m above floor.

Figure 6.25: Room 1 - transient CO_2 volume fraction profiles predicted by FireFoam compared with experimental data [3].

6.5 Room 3

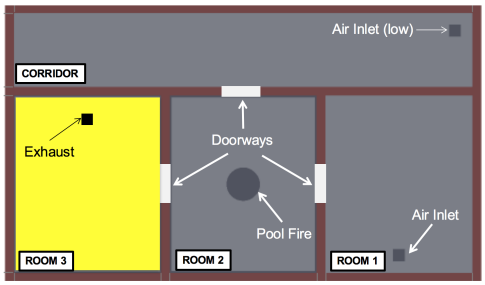

Figure 6.26: PRISME Integral Test 4 - Room 3 location.

In this section, a detailed comparison between the numerical results and experimental data will be conducted for Room 3. This compartment contains the only outlet out of the four compartments.

6.5.1 Temperature

Table 6.8: Room 3 - temperature comparison between FireFOAM, FDS, and experimental data in the steady-state region.

	Height (m)	**Exp**	**FireFOAM**		**FDS**	
			Temp	**Deviation**	**Temp**	**Deviation**
Room 3	1.05 m	449 K	363 K	19.2 % / 86 K	525 K	16.9 % / 76 K
	2.05 m	511 K	404 K	20.9 % / 107 K	557 K	8.9 % / 45 K
	3.05 m	554 K	452 K	18.4 % / 102 K	593 K	6.9 % / 38 K
	3.90 m	638 K	541 K	15.2 % / 97 K	650 K	1.8 % / 11 K

For FireFOAM, temperature is generally under-predicted throughout Room 3, as shown in Fig. 6.27 and and Table 6.8 for the transient and steady-state temperature profiles, respectively. In the numerical results, the temperature is under-predicted beyond 200 s for all four heights. Within the steady-state region, for the heights of 1.05 m, 2.05 m, 3.05 m, and 3.90 m, the temperature under-predictions are 86 K (19.2 %), 107 K (20.9 %), 102 K (18.4 %), and 97 K (15.2 %), respectively. As described in Section 6.3, FireFOAM over-predicts the fuel consumption rate, leading to premature combustion in the fire room. Consequently, the temperature in Room 3 is expected to be slightly under-predicted because it is farther downstream from the fuel source. In addition, although the magnitude of the first temperature peak occurring at 350 s is not captured by FireFOAM, the trend is very well captured. As for the second temperature peak, occurring at 1350 s, the magnitude is well reproduced by FireFOAM, but the duration of the temperature peak is much shorter than what was observed in the experimental data. Similar to the observation in Room 2, the short duration of the temperature peak in Room 3 is due to the depletion of oxygen. As shown in Fig 6.28b, oxygen is depleted at approximately 1300 s for the height of 3.2 m. The temperature peak occurs when the oxygen concentration within that region reaches a critical level. Consequently, due to oxygen depletion, a rapid decline of temperature would shortly follow the temperature peak, leading to the short duration of the second temperature peak.

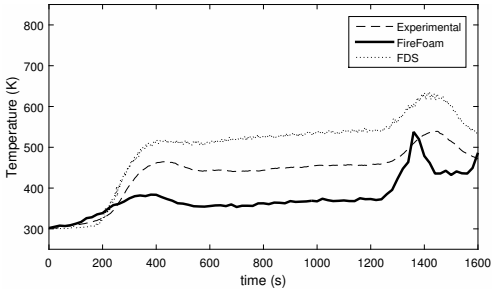

(a) Height = 1.05 m above floor.

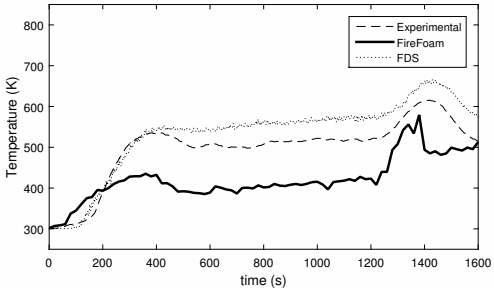

(b) Height = 2.05 m above floor.

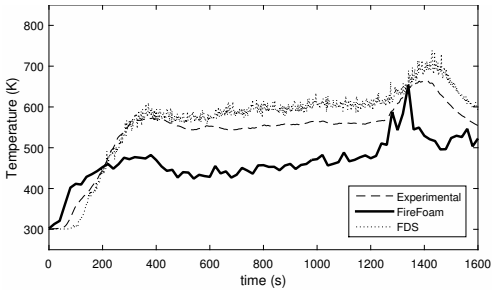

(c) Height = 3.05 m above floor.

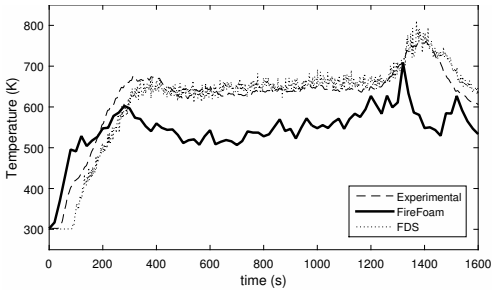

(d) Height = 3.90 m above floor.

Figure 6.27: Room 3 - transient temperature profiles predicted by FireFoam compared with experimental data [3].

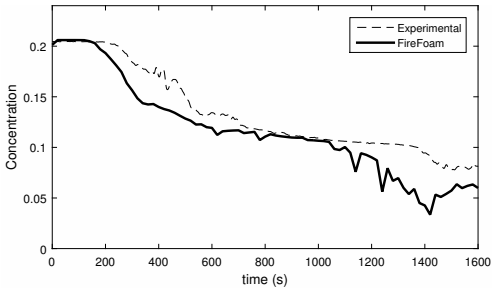

(a) Height = 0.76 m above ground.

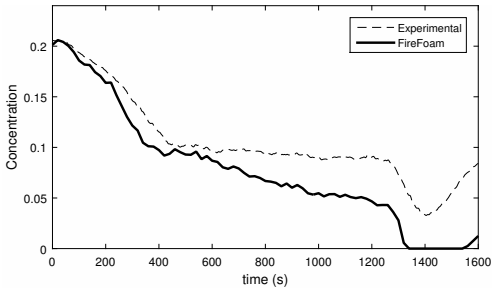

(b) Height = 3.20 m above ground.

Figure 6.28: Room 3 - transient O_2 volume fraction profiles predicted by FireFoam compared with experimental data [3].

The agreement between the FDS results and the experimental data is excellent for the two higher heights (3.05 m and 3.90 m). The initial region, steady-state region, and temperature peak occurring at 1400 s are well captured. For the two lower heights, at 1.05

m and 2.05 m, the transient temperature profiles follow the experimental data trend in the initial region, but beyond the initial region there are up to 76 K (43.5 %) and 45 K (19.3 %) over-predictions for the 1.05 m and 2.05 m heights, respectively. In comparison to the FireFOAM simulations, FDS is better at capturing the transient temperature profile at 2.05 m, 3.05 m, and 3.90 m, and both FireFOAM and FDS poorly estimate the temperature at 1.05 m.

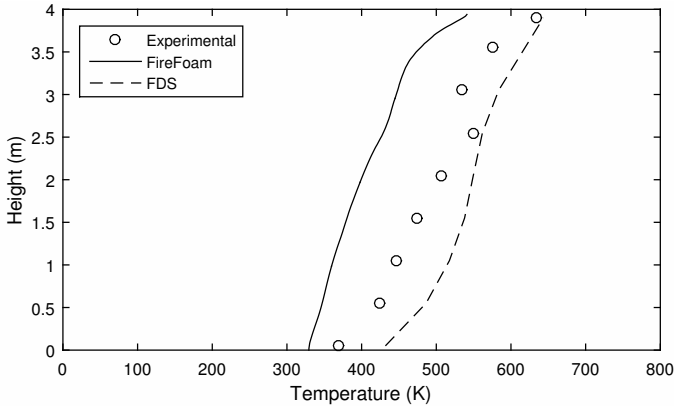

Figure 6.29: Steady-state temperature in Room 3.

6.5.2 CO_2 volume fraction

Table 6.9: Room 3 - CO_2 comparison between FireFOAM, FDS, and experimental data in the steady-state region.

	Height (m)	**Exp**	**FireFOAM**		**FDS**	
			CO_2	**Deviation**	**CO_2**	**Deviation**
Room 3	0.84 m	0.0577	0.0665	15.3 % / 0.0088	0.0362	37.1 % / 0.0214
	3.27 m	0.0931	0.0957	2.7 % / 0.0025	0.0547	41.2 % / 0.0383

As shown in Fig. 6.30, FireFOAM is gives excellent predictions of CO_2 volume fraction, whereas FDS under-predicts these CO_2 concentrations at both heights significantly. As shown in Table 6.9, FDS under-predicts the steady-state CO_2 concentration by 37.1 % and 41.2 % for the heights of 0.84 m and 3.27 m, respectively. As for FireFOAM, the steady-state CO_2 concentration are relatively close to the experimental data, with over-predictions by 15.3 % and 2.7 % for the heights of 0.84 m and 3.27 m, respectively. The flow of heat

and combustion products into this compartment are a result of the flow from the adjacent compartment and therefore inaccuracies in the flow field or fuel consumption rate would cause an error in species predictions in this outlet room.

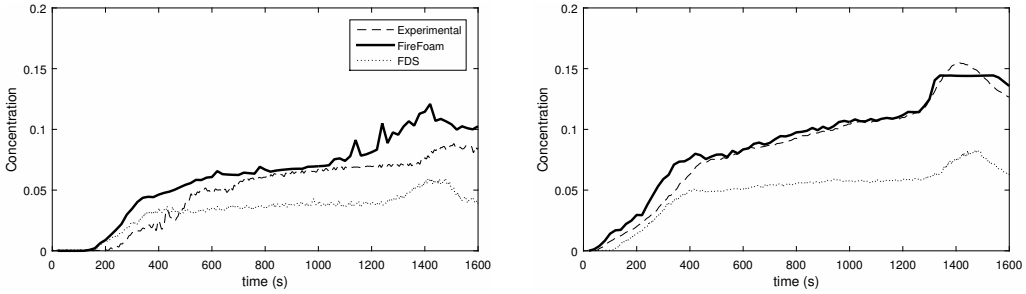

(a) Height = 0.76 m above floor. (b) Height = 3.20 m above floor.

Figure 6.30: Room 3 - transient CO_2 volume fraction profiles predicted by FireFoam compared with experimental data [3].

6.6 Corridor

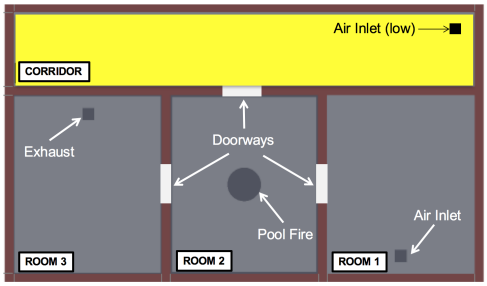

Figure 6.31: PRISME Integral Test 4 - Corridor location.

In this section, a detailed comparison between the numerical results and experimental data will be conducted for the Corridor. This compartment contains the weaker air inlet and is very long and narrow in arrangement. Similar to Room 3, the majority of the species and heat transfered into this room come from the Room 2 (fire room).

6.6.1 Temperature

The transient temperature profile is shown as a function of time in Fig. 6.32. Other than the minor under-prediction of temperature within the steady-state region at 3.05 m (Fig. 6.33) and minor over-prediction of the temperature peak occurring at 1350 s for all heights, the FireFOAM temperature predictions are in excellent agreement with the experimental data.

For FDS, the transient temperature profiles are in even better agreement. The steady-state temperatures are predicted very well for all heights. However, there are slight over-predictions of the temperature peak occurring at 1350 s for the three higher sensors and slight under-predictions of the temperature in the initial region for the height of 3.90 m.

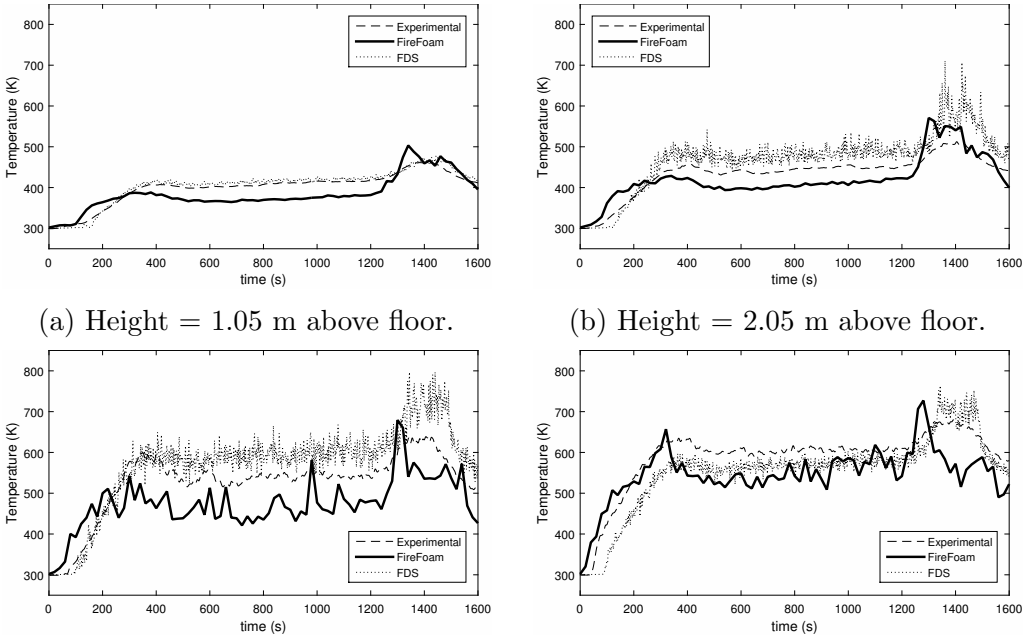

(a) Height = 1.05 m above floor.

(b) Height = 2.05 m above floor.

(c) Height = 3.05 m above floor.

(d) Height = 3.90 m above floor.

Figure 6.32: Corridor - transient temperature profiles predicted by FireFoam compared with experimental data [3].

Table 6.10: Corridor - temperature comparison between FireFOAM, FDS, and experimental data in the steady-state region.

	Height (m)	**Exp**	**FireFOAM**		**FDS**	
			Temp	**Deviation**	**Temp**	**Deviation**
Corridor	1.05 m	408 K	371 K	8.8 % / 36 K	415 K	1.7 % / 7 K
	2.05 m	444 K	406 K	8.5 % / 37 K	481 K	8.3 % / 36 K
	3.05 m	538 K	463 K	14 % / 75 K	592 K	10 % / 54 K
	3.90 m	604 K	550 K	8.9 % / 53 K	570 K	5.6 % / 33 K

As for the steady-state temperatures, as shown in Fig. 6.33 and Table 6.10, both FireFOAM and FDS predict the steady-state temperature profiles well between 0 to 2 m. Beyond 2 m, there are marginal under-predictions of temperature for FireFOAM marginal over-predictions of temperature for FDS up to 2.5 m.

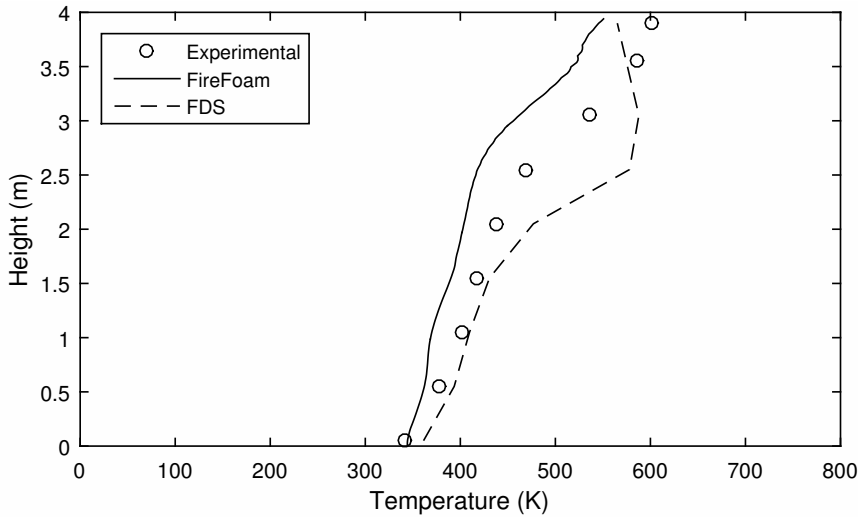

Figure 6.33: Steady-state temperature in the Corridor.

6.6.2 CO_2 volume fraction

Table 6.11: Corridor - CO_2 comparison between FireFOAM, FDS, and experimental data in the steady-state region.

	Height (m)	**Exp**	**FireFOAM**		**FDS**	
			CO_2	**Deviation**	**CO_2**	**Deviation**
Corridor	0.76 m	0.0657	0.0659	0.3 % / 0.0002	0.0652	0.8 % / 0.0005
	3.20 m	0.0715	0.0718	0.2 % / 0.0002	0.0725	1.3 % / 0.0009

For FireFOAM, as shown in Fig. 6.34, the CO_2 concentrations are very well captured in the initial region and the steady-state region. The only time period that experiences slight over-prediction of CO_2 concentrations is near the second temperature peak. As shown in Table 6.11, the prediction of CO_2 concentrations within the steady-state region are within 0.3 % and 0.2 % for the heights of 0.76 m and 3.20 m, respectively.

The FDS transient CO_2 concentrations are in even better agreement with the experimental data than FireFOAM. In addition to great predictions in the initial region and steady-state region, FDS captures the CO_2 peak occurring at 1350 s slightly better than FireFOAM at both heights.

Nevertheless, the CO_2 concentrations obtained by both numerical softwares are relatively similar and there are no major advantages to any of the two codes. Both FireFOAM and FDS are able to predict the CO_2 concentration in this compartment very well.

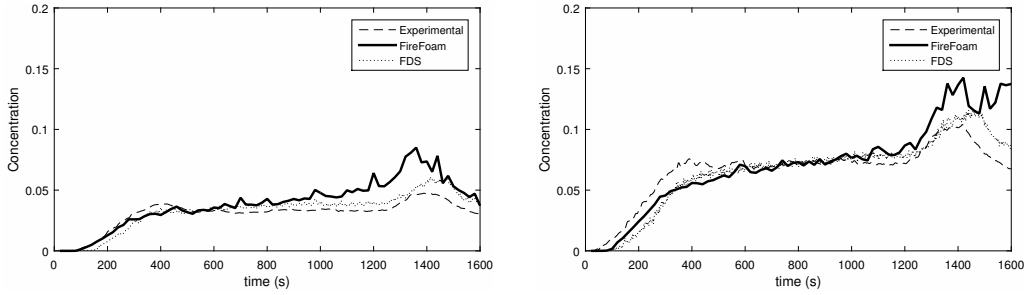

(a) Height = 0.84 m above floor. (b) Height = 3.27 m above floor.

Figure 6.34: Corridor - transient CO_2 volume fraction profiles predicted by FireFoam compared with experimental data [3].

6.7 Summary

In summary, the results of this numerical study show that FireFOAM is comparable to FDS and has the capabilities to predict the flow parameters within multi-compartment fire scenarios relatively well. The temperature, CO_2 species concentration, doorway velocity, and pressure simulation results were compared with the experimental data with success. Most of the flow parameters (pressure, species concentration, temperature, and velocity) were well predicted in most of the compartments for both numerical codes. FireFOAM showed a tendency to under-predict the temperatures slightly in most of the sensors considered. In contrast, FDS appeared to generally slightly over-predict the temperatures in most of the sensors considered.

Chapter 7

Conclusions

Overall, the present FireFoam simulation is comparable to the FDS study. Both numerical codes have predicted the transient profiles of temperature, species, pressure, and doorway velocity well. For FireFOAM, the predictions of temperature and species are predicted particularly well for Room 1 and the Corridor. For Room 2 (room where the pool fire is initiated), there are under-estimations of temperature for the bottom three sensors, possibly due to errors in modeling the residence time that led to a very high fuel consumption rate. The largest under-prediction of temperature is observed in Room 3, possibly due to turbulence modeling and combustion modeling errors. For FDS, the temperature and species are predicted well for all compartments, particularly at the lower heights. As for the pressure predictions, the trends are very well captured by FireFOAM, but the magnitudes of the pressure peaks are slightly under-predicted. FDS is better able to capture the fluctuations and pressure peaks, but the steady-state region is slightly over-predicted. Finally, for the doorway velocity predictions, both FireFOAM and FDS are able to capture them very well for most sensors considered.

In general, FDS appears to obtain better predictions than FireFOAM for the temperature in most of the compartments. This can be explained by the difference in modeling of the residence time in the EDC combustion model. FireFOAM only considers the turbulent kinetic energy and turbulent dissipation rate in its formulation of the residence time, whereas FDS considers molecular diffusion, turbulent advection, buoyancy acceleration, chemical reaction rate, and flame rate in its formulation of the residence time.

In terms of recommendations and future work, there are several items that could potentially improve the accuracy of the FireFOAM predictions for this specific case. Firstly, the inclusion of a sophisticated ventilation network could potentially improve pressure predictions. Secondly, more advanced chemistry models (e.g 2-step chemistry) could be

considered to obtain more reliable species and temperature prediction. Thirdly, the consideration of factors that FDS included in the formulation of residence time could potentially improve the fuel consumption rate in FireFOAM. In addition, other radiation models that may be more applicable to this specific experiment should be reviewed. Furthermore, studies with finer mesh sizes should be investigated. Finally, other sophisticated combustion models should be examined to improve the prediction of temperature and species near and away from the fuel surface.

References

[1] A. Trouve and Y. Wang, "Large eddy simulation of compartment fires," *Int. J. Comput. Fluid D.*, vol. 24, pp. 449–466, 2010.

[2] L. Gay, B. Sapa, and F. Nmira, "Magic and code_saturne developments and simulations for mechanically ventilated compartment fires," *Fire Safety J.*, vol. 62, pp. 161–173, 2013.

[3] H. Prétrel and G. Boioli, "Prisme integral programme," *IRSN (Institute for Radiological Protection and Nuclear Safety)*, 2010.

[4] J. L. Torero, "Special issue on prisme fire safety in nuclear facilities," *Fire Safety J.*, vol. 62, pp. 79–220, 2013.

[5] L. Audouin, L. Rigollet, H. Prétrel, W. LeSaux, and M. Röwekamp, "Oecd prisme project: Fires in confined and ventilated nuclear-type multi-compartments - overview and main experimental results," *Fire Safety J.*, vol. 62, pp. 80–101, 2013.

[6] H. P. S. Vaux, "Relative effects of inertia and buoyancy on smoke propagation in confined and forced ventilated enclosure fire scenarios," *Fire Safety J.*, vol. 62, pp. 206–220, 2013.

[7] F. Bonte, N. Noterman, and B. Merci, "Computer simulations to study interaction between burning rates and pressure variations in confined enclosure fires," *Fire Safety J.*, vol. 62, pp. 125–143, 2013.

[8] J. Wahlqvist and P. V. Hees, "Validation of fds for large-scale well-confined mechanically ventilated fire scenarios with emphasis on predicting ventilation system behavior," *Fire Safety J.*, vol. 62, pp. 102–114, 2013.

[9] M. Pelzer and W. Klein-Hebling, "Validation of cocosys pyrolysis models on oecd prisme fire experiments," *Fire Safety J.*, vol. 62, pp. 174–191, 2013.

[10] D. Drysdale, *An Introduction to Fire Dynamics Third Edition*. John Wiley & Sons, 2011.

[11] M. Lui, Y. He, and V. Beck, "Application of field model and two-zone model to flashover fires in a full-scale multi-room single level building," *Fire Safety J.*, vol. 29, pp. 1–25, 1997.

[12] F. Global, "Firefoam," *http://code.google.com/p/firefoam-dev/*.

[13] Y. Wang, P. Chatterjee, and J. L. de Ris, "Large eddy simulation of fire plumes," *Proceedings of the Combustion Institute*, vol. 33, p. 24732480, 2011.

[14] Z. Chen, J. X. B. Wen, and S. Dembele, "Large eddy simulation of a medium-scale methanol pool fire using the extended eddy dissipation concept," *Int. J. of Heat Mass Tran.*, vol. 70, p. 389408, 2014.

[15] C. J. Wang, J. X. Wen, and Z. B. Chen, "Simulation of large-scale lng pool fires using firefoam," *Combust. Sci. Tech.*, vol. 186, pp. 1632–1649, 2014.

[16] K. McGrattan, B. Klein, S. Hostikka, and J. Floyd, "Fire dynamics simulator (version 6) users guide," *National Institute of Standards and Technology Report*, vol. NIST Special Publication 1019, 2012.

[17] G. V. Hadjisophocleous, N. Benichou, and A. S. Tamim, "Literature review of performance-based fire codes and design environment," *J. Fire Protect. Eng.*, vol. 9, pp. 12–40, 1998.

[18] A. Bwalya, "An overview of design fires for building compartments," *Fire Technol.*, vol. 44, pp. 167–184, 2008.

[19] V. Babrauskas, "Fire modeling tools for fse: Are they good enough?," *J. Fire Protect. Eng.*, vol. 8, pp. 87–93, 1995.

[20] W. W. Jones, R. D. Peacock, G. P. Forney, and P. A. Reneke, "Consolidated model of fire growth and smoke transport (version 6)," *National Institute of Standards and Technology Report*, 2009.

[21] C. Zhang, *Fire Modeling*. Springer, 2015.

[22] W. C. Park, "A study of pyrolysis of charring materials and its application to fire safety and biomass utilization," Master's thesis, University of Michigan.

[23] S. Yuan and J. Zhang, "Large eddy simulation of compartment fire with solid combustibles," *Fire Safety J.*, vol. 44, pp. 349–362, 2009.

[24] H. Pretel, W. Saux, and L. Audouin, "Determination of the heat release rate of large scale hydrocarbon pool fires in ventilated compartments," *Fire Safety J.*, vol. 62, pp. 192–205, 2013.

[25] S. R. Turns, *An Introduction to Combustion - Concepts and Applications - Second Edition*. McGraw-Hill, 2000.

[26] K. Remesh and K. H. Tan, "Performance comparison of zone models with compartment fire tests," *Adv. Struct. Eng.*, vol. 17, pp. 993–1009, 2014.

[27] R. D. Peakcock, P. A. Reneke, R. W. Bukowski, and V. Babrauskas, "Defining flashover for fire hazard calculations," *Fire Safety J.*, vol. 32, pp. 331–345, 1999.

[28] E. E. Zukoski, *Combustion Fundamentals of Fire*. G. Cox Editor, Academic Press, 1995.

[29] A. Trouvé, "Cfd modeling of large-scale pool fires," *The Second International Energy 2030 Conference*, 2008.

[30] J. Carlsson, *An Introduction for Fire Safety Engineers*. Lund Institute of Technology, 1999.

[31] M. Rudman and H. M. Blackburn, "Direct numerical simulation of turbulent non-newtonian flow using a spectral element method," *Appl. Math Model.*, vol. 30, pp. 1229–1248, 2006.

[32] J. Mathieu and J. Scott, *An Introduction to Turbulent Flow*. Cambridge University Press, 2000.

[33] S. B. Pope, *Turbulent Flows*. Cambridge University Press, 2000.

[34] M. Yaga, H. Endo, T. Yamamoto, H. Aoki, and T. Miura, "Modeling of eddy characteristic time in les for calculating turbulent diffusion flame," *Heat Mass Transfer*, vol. 45, pp. 2343–2349, 2002.

[35] Y. Zhiyin, "Large-eddy simulation: Past, present and the future," *Chinese J. Aeronaut.*, vol. 28, pp. 11–24, 2015.

[36] R. Friedman, "An international survey of computer models for fire and smoke," *J. Fire Protect. Eng.*, vol. 4, pp. 81–92, 1992.

[37] K. N. C. Bray, P. A. Libby, G. Masuya, and J. B. Moss, "Turbulence production in premixed turbulent flames," *Combust. Sci. Tech.*, vol. 25, pp. 127–140, 1981.

[38] F. E. Marble and J. E. Broadwell, "The coherent flame model for turbulent chemical reactions," *Project Squid Technical Report TRW-9-PU*, 1977.

[39] D. B. Spalding, "Mixing and chemical reaction in steady confined turbulent flames," *Symposium (International) on Combust.*, vol. 13, pp. 649–657, 1971.

[40] P. A. Libby and K. N. C. Bray, "Implications of the laminar flamelet model in premixed turbulent combustion," *Combust. Flame*, vol. 39, pp. 33–41, 1980.

[41] H. K. Versteeg and W. Malalasekera, *An introduction to computational fluid dynamics: the finite volume method*. Prentice Hall, 2007.

[42] E. Hopf, "Statistical hydromechanics and functional calculus," *J. Ration. Mech. Anal.*, vol. 1, pp. 87–123, 1952.

[43] A. Y. Klimenko, "Multicomponent diffusion of various scalars in turbulent flow," *Fluid Dyn.*, vol. 25, pp. 327–333, 1990.

[44] K. J. Bathe, *Computational Fluid and Solid Mechanics*. Elsevier Science, 2003.

[45] B. Lilleberg, D. Christ, I. S. Ertesvag, K. E. Rian, and R. Kneer, "Numerical simulation with an extinction database for use with the eddy dissipation concept for turbulent combustion," *Flow Turbul. Combust.*, vol. 91, pp. 319–346, 2013.

[46] B. Magnussen and B. Hjertager, "On mathematical modeling of turbulent combustion with special emphasis on soot formation and combustion," *Symposium (International) on Combust.*, vol. 16, pp. 719–729, 1977.

[47] L. Kjaldman, A. Brink, and M. Hupa, "Micro mixing time in the eddy dissipation concept," *Combust. Sci. Tech.*, vol. 154, pp. 207–227, 1999.

[48] D. Veynante and L. Vervisch, "Turbulent combustion modeling," *Prog. Energ. Combust.*, vol. 28, pp. 193–266, 2002.

[49] A. Shiehnejadhesar, R. Mehrabian, R. Scharler, G. M. Goldin, and I. Obernberger, "Development of a gas phase combustion model suitable for low and high turbulence conditions," *Fuel*, vol. 126, pp. 177–187, 2014.

[50] R. W. Bilger, "Turbulent diffusion flames," *Annu. Rev. Fluid Mech.*, vol. 21, pp. 101–135, 1989.

[51] X. S. Bai and L. Fuchs, "Sensitivity study of turbulent reacting flow modeling," *AIAA J.*, vol. 33, pp. 1857–1864, 1995.

[52] J. Collazo, J. Porteiro, D. Patino, J. L. Miguez, E. Granada, and J. Moran, "Simulation and experimental validation of a methanol burner," *Fuel*, vol. 88, pp. 326–334, 2009.

[53] J. Buckmaster, P. Clavin, A. Linan, M. Matalon, N. Peters, G. Sivashinsky, and F. A. Williams, "Combustion theory and modeling," *P. Combust. I.*, vol. 30, pp. 1–19, 2005.

[54] *Software availble at http://www.openfoam.org.*

[55] S. Menon, P. Yeung, and W. Kim, "Effect of subgrid models on the computed interscale energy transfer in isotropic turbulence," *Comput. Fluids*, vol. 25, pp. 165–180, 1996.

[56] J. W. Deardorff, "Stratocumulus-capped mixed layers derived from a three-dimensional model," *Bound.-Layer Meteor.*, vol. 18, pp. 495–527, 1980.

[57] D. Hosser and V. Hohm, "Application of a new model for the simulation of coupled heat transfer processes during fires to safety relevant objects in nuclear facilities," *Fire Safety J.*, vol. 62, pp. 144–160, 2013.

[58] B. Gautier, "Fire zone model magic: The validation and verification principles," *International Collaborative Project to Evaluate Fire Models for NPP Applications*, 2002.

[59] F. Archambeau, N. Mechitoua, and M. Sakiz, "Code_saturne: a finite volume code for the computation of turbulent incompressible flows - industrial applications," *Int. J. Finite*, 2004.

[60] H. J. Allenlein, S. Arndt, W. Klein-Heßling, S. Schwarz, C. Spengler, and G. Weber, "Cocosys: Status of development and validation of the german containment code system," *Nucl. Eng. Des.*, vol. 238, pp. 872–889, 2008.

[61] S. Melis, P. Querre, and L. Picciardi, "Physical modeling of sylvia v1.4, technical note," 2009.

[62] R. Barlow, "Scalar profiles and no formation in laminar opposed-flow partially premixed methane/air flames," *Combust. Flame*, vol. 127, pp. 2102–2118, 2001.

[63] W. Grosshandler, "Radcal: A narrow-band model for radiation calculations in a combustion environment," *National Institute of Standards and Technology (U.S.)*, vol. NIST Technical Note 1402, 1993.

[64] B. J. McBride, S. Gordon, and M. A. Reno, "Coefficients for calculating thermodynamic and transport properties of individual species.," *NASA technical memorandum 4513*, 1993.

[65] M. W. Chase, *NIST-JANAF Thermochemical Tables*. J. Phys. Chem. Ref. Data, 1998.